Photodriven germanium hole qubit

Bashab Dey ⬤ and John Schliemann

Institute of Theoretical Physics, University of Regensburg, Regensburg, Germany

Hole qubits in germanium quantum dots are promising candidates for coherent control and manipulation of the spin degree of freedom through electric dipole spin resonance. We theoretically study the time dynamics of a single heavy-hole qubit in a laser-driven planar germanium quantum dot confined laterally by a harmonic potential in the presence of linear and cubic Rashba spin-orbit couplings and an out-of-plane magnetic field. We obtain an approximate analytical formula of the Rabi frequency using a Schrieffer-Wolff transformation and establish a connection of our model with the ESDR results obtained for this system. For stronger beams, we employ different methods such as unitary transformation and Floquet theory to study the time evolution numerically. We observe that high radiation intensity is not suitable for the qubit rotation due to the presence of high-frequency noise superimposed on the Rabi oscillations. We display the Floquet spectrum and highlight the quasienergy levels responsible for the Rabi oscillations in the Floquet picture. We study the interplay of both the types of Rashba couplings and show that the Rabi oscillations, which are brought about by the linear Rashba coupling, vanish for typical values of the cubic Rashba coupling in this system.

I. INTRODUCTION

Qubit is the basic unit of quantum information. The search for materials where qubits can be fast-operated, efficiently controlled, and well shielded from the environment has been at the forefront of research. Solid-state spin qubits, such as in Si, Ge, and III-V semiconductor heterostructures, have attracted immense attention in recent times as nanometer-scale quantum devices can be lithographically fabricated onto them, creating an isolated environment for the spins to achieve long coherence times [1–4]. Furthermore, technological advancements in microelectronics and production of high-quality Si hold great prospect of building a scalable semiconductor platform to develop quantum computers which may host millions of qubits [5,6].

The Zeeman-split electronic spin states are suitable candidates for single and multiqubit operations, as proposed by Loss and DiVincenzo [7]. Single qubit gates such as *Pauli* gates have been realized in Si and GaAs by inducing Rabi oscillations between the spin-up and -down states with the help of electron spin resonance (ESR) [8–12]. However, ESR offers experimental roadblocks from the point of view of scaling as magnetic fields are difficult to localize in miniature landscapes. However, electrical driving is easier to implement locally through the application of ac voltage across the *in situ* gate electrodes. Modulation of *g*-tensor [13–17], slanting-Zeeman field ESR [18–21], and electric dipole spin resonance (EDSR) [22,23] have proved to be reliable techniques for achieving coherent qubit control through pure electrical drives. Among these, EDSR is of particular interest as it harnesses the spin-orbit coupling (SOC) of the material to perform the qubit rotations. The mechanism of EDSR has been extensively studied over the years in quantum wells [24], planar quantum dots with electron- [25] or hole-qubits [26], TMD monolayers [27], and double quantum dots [28]. The

electronic spin-qubits in 2D GaAs quantum dot [22] and InSb nanowire [23] have successfully exhibited single-spin EDSR.

The electron spin qubits are prone to decoherence and relaxations due to interaction with phonons [29–32] in the presence of SOC and contact-hyperfine interaction with the sea of nuclear spins [33–35]. The latter can be substantially minimized in group IV semiconductors such as Si and Ge as they can be engineered into nuclear-spin free materials by isotopic purification [36–38]. In recent times, hole spin-qubits have emerged as viable alternatives to the electronic counterparts [39]. The suppressed hyperfine interaction due to the *p*-nature of the hole wave function leads to longer coherence times [40–43]. Moreover, the valley degeneracy which stands as an obstacle in using Si electrons as spin-qubits [44], is absent for holes. The most attractive feature is, however, the stronger SOC of holes as compared to that of conduction electrons, which facilitates faster EDSR [26]. However, it can also lead to stronger decoherence through spin-phonon interactions [45].

Although Si might appear to be the natural choice for hole spin-qubits, it is Ge that provides some of the most desirable features for qubit control [46]. The smaller effective mass of holes in Ge [47] relaxes nanofabrication requirements, as the quantum dots are larger than in Si. Since Ge is heavier than Si, it has stronger SOC [48] which is desirable for faster qubit operations. Single-hole qubit rotations have been successfully demonstrated in planar Ge quantum wells and nanowires using EDSR [49–52]. The 2D holes of Ge exhibit *p-cubic* Rashba SOC [53,54] consisting of cubic- ($\propto p_+ p_- p_+ \sigma_+ +$ H.c.) and spherically symmetric terms ($\propto p_+^3 \sigma_- +$ H.c.), out of which the latter dominates. The Dresselhaus SOC is absent due to bulk-inversion symmetry of the crystal. Several theoretical studies have attributed the EDSR in planar Ge quantum dots to the cubic-symmetric component of the SOC [52,55] in the presence of an

out-of-plane magnetic field. The electrical operation of planar Ge hole spin qubits in an in-plane magnetic field has also been studied theoretically [56]. However, it has been recently argued that the cubic-symmetric component is negligibly small and a *p-linear direct* Rashba SOC, which exists in [001]-oriented Ge/Si quantum wells, is indeed responsible for the EDSR [57]. Its origins are attributed to the local C_{2v} interface [58–61] and is deduced by performing atomistic pseudopotential method calculations [57,62]. Further studies have also claimed the existence of a *p*-linear Dresselhaus SOC in these heterostructures originating from heavy-hole/light-hole mixings [63]. A specific kind of *p*-linear Rashba SOC can also be induced by moving the dot across inhomogeneous strain fields, which along with *g*-factor modulations results in faster Rabi rotations [64]. Inhomogenous and inseparable electric fields can also lead to a different type of SOC mechanism that supports hole manipulation with in-plane magnetic fields [65].

In the past two decades, there have been significant developments in intense-ultrafast laser spectroscopy [66–68], which gave birth to Floquet engineering. The previous works on EDSR with hole spin-qubits dealt with the application of electric pulses through gate electrodes only. The study of EDSR with laser pulses or optical EDSR is still missing. Second, the EDSR problem was only treated perturbatively and the effects of stronger electric fields were not addressed. Third, the previous works did not take into account the effect of simultaneous presence of both linear and cubic Rashba SOC in determining the nature of EDSR. In this work, we make a comprehensive study of all the above aspects by studying EDSR of 2D HH states of Ge driven by a circularly polarized laser beam. We consider the dominant forms of SOC in this system viz. the *p*-linear and the spherically symmetric component of *p*-cubic Rashba SOC. We show that the effect of laser field is equivalent to that of the usual gate-driven EDSR setup. For small linear Rashba parameter and weak driving (perturbative limit), we perform a Schrieffer-Wolff transformation to obtain approximate analytical expressions of the Rabi frequency and Rabi transition probabilities. For realistic system parameters, the Rabi frequency turns out to be of the order of megahertz. We discuss the dependence of the maximum transition probability and width of the resonances on the magnetic field strength, driving frequency and Rashba parameter. For stronger driving and larger Rashba strengths, we resort to numerical methods. In the presence of either of the Rashba couplings, we exploit the "rotational" symmetries of the system to derive a unitary transformation that converts the driven Hamiltonian into a static one, making the numerical computation of the time-evolved state easier. We observe a high-frequency component superimposed on the resonant Rabi oscillations for larger amplitudes of radiation, which the perturbation theory does not capture. When both the Rashba couplings are present, we use Floquet theory to numerically calculate the time evolution. We study the interplay of both the couplings and observe that large and realistic values of the cubic Rashba coupling drives the system out of resonance and effectively destroys the Rabi oscillations. We also show that the Rabi frequency is equal to quasienergy gap between two adjacent Floquet levels, which increases with the radiation amplitude.
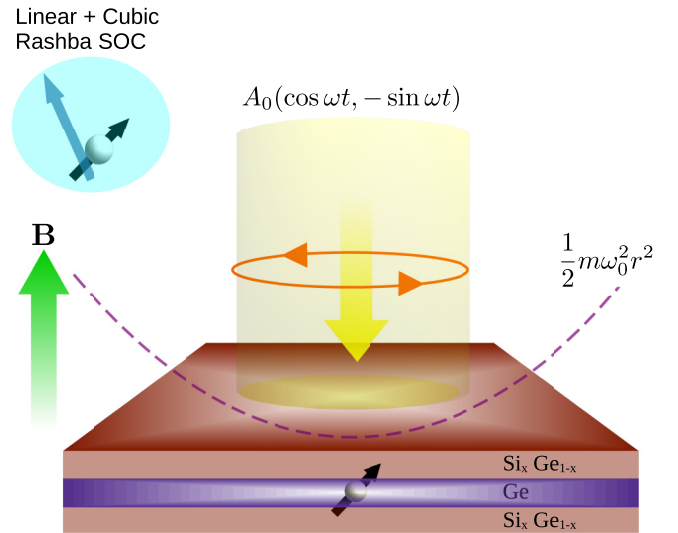

FIG. 1. Schematic diagram of the model.

The paper is organized as follows. In Sec. II, we discuss the theoretical model of the planar Ge quantum dot. In Sec. III, we derive the interaction Hamiltonian of the laser beam with the hole qubit. In Sec. IV A, we study relation between time evolution of the driven system in different gauges. Section IV B deals with analytical formalism to obtain the Rabi frequency of the system when the SOC and drive are treated perturbatively. In Sec. IV C, we discuss the numerical methods such as unitary transformation and Floquet theory use to solve the Schrödinger equation. In Sec. V, we present and analyze the results of our study for realistic system parameters and laser strengths in the presence of either or both types of SOC in this system. Finally, we conclude our results in Sec. VI.

II. MODEL

In groups IV and III–V semiconductors, the hole states lie close to the Γ point of valence band of these materials and have effective spin $J = 3/2$. These states can be described by the 4×4 Luttinger Hamiltonian [69]. In 2D quantum wells confined along the growth direction, the heavy-hole (HH) states (spin $\pm 3/2$) split apart from the light-hole (LH) ones (spin $\pm 1/2$) with a higher energy. The splitting depends on the well thickness (say d) and varies as d^{-2}. We consider a 2D HH-gas of Ge confined electrostatically in the lateral direction and subjected to a magnetic field perpendicular to the 2D plane ($\mathbf{B} = B\hat{z}$) as shown in Fig. 1. The confinement can be modeled by a parabolic potential $U(x, y) = m\omega_0^2(x^2 + y^2)/2$, where $\omega_0 = \hbar/(ml_0^2)$ with l_0 being the confinement length-scale (approximated as radius of the dot) and m being the effective heavy hole mass. Including the SOC effects, the Hamiltonian of the HH states in the out-of-plane magnetic field can be written as

$$H_0 = \frac{P^2}{2m} + U(x, y) - \frac{1}{2}g_\perp \mu_B B\sigma_z + i\alpha_c(P_-^3\sigma_+ - P_+^3\sigma_-)$$
$$- i\alpha_l(P_-\sigma_+ - P_+\sigma_-), \qquad (1)$$

where $\mathbf{P} = \mathbf{p} - |e|\mathbf{A}_B(\mathbf{r})$, $\mathbf{A}_B(\mathbf{r}) = B(-y, x)/2$, $\sigma_\pm = (\sigma_x \pm i\sigma_y)/2$, and $P_\pm = P_x \pm iP_y$. The parameter

$\alpha_c = 3\gamma_0\alpha_R\langle E_z\rangle/(2\Delta m_e)$ is the cubic Rashba SOC strength (corresponding to the dominant spherically symmetric contribution) which is directly proportional to the average electric field at the interface $\langle E_z\rangle$ and inversely proportional to HH-LH splitting Δ. Here, m_e is the bare electron mass, α_R the coupling constant, γ_0 a Luttinger parameter and $g_\perp$ the out-of-plane component of the g-factor tensor. The parameter γ_0 is equal to the Luttinger parameters γ_2 and γ_3 within the spherical approximation of the Luttinger Hamiltonian, i.e., $\gamma_0 = \gamma_2 \approx \gamma_3$ [70]. The parameter α_l denotes the newly claimed linear Rashba SOC strength [57]. The Rashba couplings can be controlled either by changing the interfacial dc electric field, the well thickness or both. When the Rashba couplings are tuned to zero, i.e., $\alpha_l = \alpha_c = 0$, the Hamiltonian is exactly solvable using the following coordinate transformations [31]:

$$x = \frac{1}{\sqrt{2\Omega}}(\sqrt{\omega_1}q_1 + \sqrt{\omega_2}q_2), \tag{2}$$

$$y = \frac{1}{m\sqrt{2\Omega}}\left(\frac{p_1}{\sqrt{\omega_1}} - \frac{p_2}{\sqrt{\omega_2}}\right), \tag{3}$$

$$p_x = \sqrt{\frac{\Omega}{2}}\left(\frac{p_1}{\sqrt{\omega_1}} + \frac{p_2}{\sqrt{\omega_2}}\right), \tag{4}$$

$$p_y = m\sqrt{\frac{\Omega}{2}}(-\sqrt{\omega_1}q_1 + \sqrt{\omega_2}q_2), \tag{5}$$

where $[q_i, q_j] = [p_i, p_j] = 0$, $[q_i, p_j] = i\hbar\delta_{i,j}$ and the constants are defined as $\omega_{1,2} = \Omega \pm \omega_c/2$, $\Omega = \sqrt{\omega_0^2 + \omega_c^2/4}$, $\omega_c = |e|B/m$, and $\omega_z = g_\perp\mu_B B/\hbar$. It is to be noted that for holes, $\omega_{1,2}$ have their signs exchanged when compared to those defined in Ref. [31]. Upon transforming, the SOC-free Hamiltonian in the new coordinates can be written as a sum of two uncoupled harmonic oscillators with Zeeman coupling

$$H_{FD} = \frac{p_1^2}{2m} + \frac{1}{2}m\omega_1^2 q_1^2 + \frac{p_2^2}{2m} + \frac{1}{2}m\omega_2^2 q_2^2 - \frac{\hbar\omega_z}{2}\sigma_z. \tag{6}$$

Using the ladder operators

$$\hat{a}_{1,2} = \sqrt{\frac{m\omega_{1,2}}{2\hbar}}\left(q_{1,2} + i\frac{p_{1,2}}{m\omega_{1,2}}\right) \tag{7}$$

and

$$\hat{a}_{1,2}^\dagger = \sqrt{\frac{m\omega_{1,2}}{2\hbar}}\left(q_{1,2} - i\frac{p_{1,2}}{m\omega_{1,2}}\right), \tag{8}$$

the Hamiltonian can be cast as

$$H_{FD} = \hbar\omega_1\left(\hat{n}_1 + \frac{1}{2}\right) + \hbar\omega_2\left(\hat{n}_2 + \frac{1}{2}\right) - \frac{\hbar\omega_z}{2}\sigma_z, \tag{9}$$

where $\hat{n}_i = \hat{a}_i^\dagger\hat{a}_i$ is the number operator. Its eigenstates are the well-known Fock-Darwin (FD) levels with energies $E_{n_1,n_2,s} = \hbar\omega_1(n_1 + 1/2) + \hbar\omega_2(n_2 + 1/2) - \hbar\omega_z s/3$ and eigenvectors $|n_1, n_2, s\rangle = \Phi_{n_1}(q_1\sqrt{m\omega_1/\hbar})\Phi_{n_2}(q_2\sqrt{m\omega_2/\hbar})|s\rangle$, where $s = \pm 3/2$. Here, $\Phi_n(...)$ is the nth excited state of the harmonic oscillator in the specified coordinates. Therefore, on tuning $\alpha_{c,l} \to 0$, we get pure localized spin states which can be used as qubits.

For finite $\alpha_{c,l}$, the last two terms of Eq. (1), representing the Rashba interaction H_R, can be rewritten as

$$H_R = H_R^{(C)} + H_R^{(L)}, \tag{10}$$

where

$$H_R^{(C)} = \alpha_c(m\hbar)^{3/2}[(f_+\hat{a}_1^\dagger + f_-\hat{a}_2)^3\sigma_+ + \text{H.c.]} \tag{11}$$

and

$$H_R^{(L)} = \alpha_l\sqrt{m\hbar}[(f_+\hat{a}_1^\dagger + f_-\hat{a}_2)\sigma_+ + \text{H.c.]}, \tag{12}$$

with

$$f_\pm = \pm\sqrt{\Omega} + \frac{\omega_c}{2\sqrt{\Omega}}. \tag{13}$$

Hence, the total Hamiltonian is $H_0 = H_{FD} + H_R^{(C)} + H_R^{(L)}$. The superscripts "C" and "L" denote cubic and linear Rashba couplings, respectively. The Rashba interactions couple the FD levels with different spin quantum numbers and hence spin is no longer a conserved quantity. The exact eigenstates of the system in the presence of the Rashba coupling(s) are unknown and hence perturbation theory is often used to study the physics of these systems. For very small Rashba strengths, the FD levels can still be considered as approximate energy levels of the system as the first order correction in energy due to the Rashba couplings are zero. The first order corrections to the energy eigenstates are however nonzero and states with opposite spins get mixed. For example, the cubic Rashba coupling mixes $|0, 0, -3/2\rangle$ with $|3, 0, 3/2\rangle$ up to first order in α_c while the linear Rashba coupling mixes $|0, 0, -3/2\rangle$ with $|1, 0, 3/2\rangle$ up to first order in α_l. However, for time spans much shorter than the coupling time scale, spin is approximately a good quantum number.

A. Symmetries

The system also has some continuous symmetries which can be seen from the commutator relations of angular momentum. In terms of the number operators, the orbital angular momentum operator can be written as $L_z = \hbar(\hat{n}_2 - \hat{n}_1)$. Since $[L_z, H_{FD}] = 0$, the orbital angular momentum is conserved in absence of the Rashba couplings. On defining operators

$$\hat{J}_z^{(L)} = L_z + \hbar\sigma_z/2 \text{ for } \alpha_l \neq 0, \alpha_c = 0 \tag{14}$$

and

$$\hat{J}_z^{(C)} = L_z + 3\hbar\sigma_z/2 \text{ for } \alpha_c \neq 0, \alpha_l = 0, \tag{15}$$

we get $[\hat{J}_z^{(L)}, H_{FD} + H_R^{(L)}] = 0$ and $[\hat{J}_z^{(C)}, H_{FD} + H_R^{(C)}] = 0$. This implies the presence of a rotational symmetry about z axis in the total Hilbert space (spin plus orbital) when either of the two Rashba couplings are present. As we show later, this symmetry of the Hamiltonian can be exploited to obtain the time-evolution of the system under circular driving.

III. CIRCULAR DRIVE BY LASER

A coherent laser beam of circularly polarized radiation is shone upon the hole gas normally (Fig. 1). We treat the laser beam classically by modeling it as a plane wave with electric and magnetic fields given by $\mathbf{E}(\mathbf{r}, t) = E_0[\sin(\omega t + kz), \cos(\omega t + kz), 0]$ and $\mathbf{B}(\mathbf{r}, t) = -(E_0/c)[-\cos(\omega t + kz),$

$\sin(\omega t + kz), 0]$, respectively. The effect of the electromagnetic field is incorporated into the Hamiltonian (1) through the vector and scalar potentials in two different gauges viz. velocity gauge and length gauge. It is to be noted that the ac electric field is in-plane and also averages out to zero over the time scales of qubit operations. Hence, it has no influence on the Rashba strength ($\propto \langle E_z \rangle$) in this model.

A. Velocity gauge

The most natural choice of gauge to describe plane wave radiation is the velocity gauge. In this gauge, the beam can be represented by a vector potential $\mathbf{A}_r(\mathbf{r}, t) = A_0[\cos(\omega t + kz), -\sin(\omega t + kz), 0]$ and $\phi(\mathbf{r}, t) = 0$, where $A_0 = E_0/\omega$ with E_0 being the electric field amplitude. The Hamiltonian (1) becomes periodic in time through Peierls substitution, i.e., $H(t) = H_0(\mathbf{P} - |e|\mathbf{A}_r(\mathbf{r}, t))$. So, in this gauge, the coupling with radiation is only through the vector potential. Since $z = 0$ for the hole gas, $\mathbf{A}_r(\mathbf{r}, t) \equiv \mathbf{A}_r(t) = A_0(\cos \omega t, -\sin \omega t, 0)$. The driven Hamiltonian can be decomposed as $H(t) = H_{\text{FD}} + H_R + V(t)$, where

$$V(t) = \sum_{n=-3}^{3} V_n e^{in\omega t}, \tag{16}$$

where V_n are the Fourier components whose matrix elements are given by

$$V_0 = \frac{e^2 A_0^2}{2m}, \tag{17}$$

$$V_1 = 3i\alpha_c |e| A_0 m\hbar (f_+ \hat{a}_1^\dagger + f_- \hat{a}_2)^2 \sigma_+ i\alpha_l |e| A_0 \sigma_+$$
$$+ i\frac{|e| A_0}{2m} \sqrt{m\hbar}(f_+ \hat{a}_1 + f_- \hat{a}_2^\dagger), \tag{18}$$

$$V_2 = -3\alpha_c \sqrt{m\hbar} |e|^2 A_0^2 (f_+ \hat{a}_1^\dagger + f_- \hat{a}_2)\sigma_+, \tag{19}$$

and

$$V_3 = -i\alpha_c |e|^3 A_0^3 \sigma_+. \tag{20}$$

Due to Hermiticity, the Fourier components are related as $V_{-n} = V_n^\dagger$. The forms of the matrix elements of V_n and H_R can be found in Appendix A. Since the magnetic vector lies in-plane, it does not have any Zeeman interaction with the hole spins because the 2×2 HH submatrices fulfill the property: $\mathcal{J}_x = \mathcal{J}_y = 0$ and $\mathcal{J}_z = 3\sigma_z/2$ [45,71].

The second term of V_1 and the term V_3 couple spins with the same orbital quantum numbers. It shows that Rabi transitions $|3/2\rangle \Longleftrightarrow |-3/2\rangle$ may be induced within the same orbital sector ($\Delta n_1 = \Delta n_2 = 0$) using circularly polarized light if the higher levels are decoupled. To begin with, let us consider the block of the two lowest lying FD states viz. $|0, 0, 3/2\rangle$ and $|0, 0, -3/2\rangle$ that have opposite spins:

$$H_{2\times2} = \begin{pmatrix} \frac{e^2 A_0^2}{2m} + \hbar\Omega - \frac{\hbar\omega_z}{2} & \kappa(t) \\ \kappa^*(t) & \frac{e^2 A_0^2}{2m} + \hbar\Omega + \frac{\hbar\omega_z}{2} \end{pmatrix}, \tag{21}$$

where $\kappa(t) = i\alpha_l |e| A_0 e^{i\omega t} - i\alpha_c |e|^3 A_0^3 e^{3i\omega t}$. The lowest block resembles a two-level system driven by harmonic modes

of frequencies 3ω and ω corresponding to cubic and linear Rashba SOCs, respectively. For $\omega = \omega_z/3$ and $\omega = \omega_z$, the Rabi frequencies are $2\alpha_c |e|^3 E_0^3/(\hbar\omega^3)$ and $2\alpha_l |e| E_0/(\hbar\omega)$, respectively. This shows that the vector potential of the coherent radiation can cause hole-spin resonance ($\Delta n_1 = 0$, $\Delta n_2 = 0$, $\Delta s = 3$) in the presence of Rashba SOC. However, the Rabi oscillations are killed by the coupling of this block with the higher energy levels and hence the two-level picture does not capture the physics of the complete system.

B. Length gauge

We may also choose another gauge where $\mathbf{A}_r'(\mathbf{r}, t) = (0, 0, E_0/c[x\sin(\omega t + kz) + y\cos(\omega t + kz)])$ and $\phi_r'(\mathbf{r}, t) = -E_0[x\sin(\omega t + kz) + y\cos(\omega t + kz)]$. The two gauges are related as: $\mathbf{A}_r'(\mathbf{r}, t) = \mathbf{A}_r(\mathbf{r}, t) + \nabla\Lambda(\mathbf{r}, t)$ and $\phi_r'(\mathbf{r}, t) = \phi_r(\mathbf{r}, t) - \partial_t \Lambda(\mathbf{r}, t)$, where

$$\Lambda(\mathbf{r}, t) \equiv \Lambda = (E_0/\omega)[-x\cos(\omega t + kz) + y\sin(\omega t + kz)]. \tag{22}$$

Since P_z is absent, $\tilde{A}_z$ does not couple with the static Hamiltonian. So, the coupling with radiation is only through the scalar potential $\phi_r'(\mathbf{r}, t) = -E_0(x\sin \omega t + y\cos \omega t)$ at $z = 0$, i.e., $H'(t) = H_{\text{FD}} + H_R + |e|\phi_r'(\mathbf{r}, t)$. This is called the length gauge.

The Hamiltonian in the length gauge is identical to that of an EDSR setup. For EDSR, a circularly rotating electric field $\mathbf{E} = E_0(\sin \omega t, \cos \omega t)$ is applied across the dot using two perpendicular pairs of gates. Then, the interaction of the heavy holes with the field can be written as

$$V_g(t) = -|e|\int^{\mathbf{r}} \mathbf{E} \cdot d\mathbf{r}' = -F_0(x\sin \omega t + y\cos \omega t), \tag{23}$$

where $F_0 = |e|E_0$. Hence, $V_g(t) = |e|\phi_r'(\mathbf{r}, t)$. It is to be noted that although the oscillating electric field also produces a magnetic field, its magnitude is $1/c$ times smaller the electric field and would have negligible effect on the spin dynamics. Hence, we can safely ignore the magnetic vector potential in this case [25].

Using the transformations (2) and (3) in Eq. (23), we get

$$V_g(t) = i\frac{F_0}{2}\sqrt{\frac{\hbar}{m\Omega}}(\hat{a}_1 e^{i\omega t} - \hat{a}_1^\dagger e^{-i\omega t} - \hat{a}_2 e^{-i\omega t} + \hat{a}_2^\dagger e^{i\omega t}). \tag{24}$$

The total Hamiltonian of the driven dot is $H'(t) = H_{\text{FD}} + H_R + V_g(t)$, where H_{FD} is the exactly solvable part and $H_R + V_g(t)$ is to be treated as perturbation. The perturbation does not couple the spins in the lowest energy block which are the Zeeman-split ground states (i.e., $n_1 = n_2 = 0$ orbital sector). So, spin rotations can be achieved only through the higher order transitions. For a drive of the form of Eq. (24), only the linear Rashba coupling supports EDSR. This can be explained as follows. At resonance $\omega = \omega_z$, $V_g(t)$ can cause a virtual transition with no spin flip ($\Delta n_i = \pm 1$, $\Delta s = 0$) followed by another virtual transition accompanied by a spin flip ($\Delta n_i = \pm 1$, $\Delta s = \pm 3$) mediated by the linear Rashba coupling in (10). This brings about the desired Rabi oscillations in the system even in absence of a rotating magnetic field. The cubic Rashba coupling cannot cause EDSR because the cubic terms

not couple levels with $\Delta n_i \neq \pm 1$ and hence the x-linear drive cannot cause virtual transitions back to the original level. Thus, the length gauge provides a better picture of the Rabi oscillations as compared to the velocity gauge.

IV. TIME EVOLUTION

A. Time evolution in different gauges

The Hamiltonians and the solutions of the time-dependent Schrödinger equation (TDSE) in the two gauges are related as

$$H'(t) = e^{i|e|\Lambda/\hbar} H(t) e^{-i|e|\Lambda/\hbar} - |e|\partial_t \Lambda \qquad (25)$$

and

$$|\psi'(t)\rangle = e^{i|e|\Lambda/\hbar}|\psi(t)\rangle, \qquad (26)$$

respectively, where Λ is defined in Eq. (22). From Eq. (26), it follows that

$$U'(t,0) = e^{i|e|\Lambda(\mathbf{r},t)/\hbar} U(t,0) e^{-i|e|\Lambda(\mathbf{r},0)/\hbar}. \qquad (27)$$

Clearly, the time evolution is gauge-dependent (as the Hamiltonian is gauge-dependent). To render the transition amplitudes gauge-invariant, the initial ($|i\rangle$) and final ($|f\rangle$) states must be gauge transformed in the following way [72]:

$$|i'\rangle = e^{i|e|\Lambda(\mathbf{r},0)/\hbar}|i\rangle, \qquad (28)$$

$$|f'\rangle = e^{i|e|\Lambda(\mathbf{r},t)/\hbar}|f\rangle. \qquad (29)$$

Then, we have $\langle f'|U'(t,0)|i'\rangle = \langle f|U(t,0)|i\rangle$. It is easier to study the dynamics in the length gauge because the interaction in this gauge has a lesser number of terms [Eq. (24)] than that in the velocity gauge [Eq. (16)]. So, it is to be noted that the numerical results presented in this paper are obtained using the length gauge only.

The exact analytical solutions of the TDSE cannot be obtained for this system in either of the two gauges. Since we are interested in Rabi oscillations, first, we obtain an approximate analytical expression of the Rabi frequency by treating the Rashba coupling(s) and the drive perturbatively. Second, we compute the numerical solutions and the Rabi frequencies using the methods of unitary transformation and Floquet theory.

B. Analytical formalism

An approximate analytical form of the Rabi frequency can also be obtained in the length gauge using perturbation theory. The linear Rashba coupling is off-diagonal in the FD basis as it couples blocks with orbital quantum number differing by 1, i.e., $\Delta n_i = \pm 1$. For small Rashba strengths $(\frac{\alpha_l \sqrt{m\hbar\omega_0}}{\hbar\omega_0} = \tilde{\alpha}_l \ll 1)$ as compared to the confinement energy scale $\hbar\omega_0$, we can perform a Schrieffer-Wolff (SW) transformation [25,30,73,74] to diagonalize the Hamiltonian of the dot such that the off-diagonal couplings are removed up to linear order in $\tilde{\alpha}_l$. Using the transformation, the effective two-level Hamiltonian for this system can be written as (see Appendix B for details)

$$H_{\text{eff}}(t) = \begin{pmatrix} E_1 & -i\gamma e^{i\omega t} \\ i\gamma e^{-i\omega t} & E_2 \end{pmatrix}, \qquad (30)$$

where

$$E_1 = -\frac{\hbar\omega_z}{2} - \frac{\alpha_l^2 m f_-^2}{\omega_2 + \omega_z}, \qquad (31)$$

$$E_2 = \frac{\hbar\omega_z}{2} - \frac{\alpha_l^2 m f_+^2}{\omega_1 - \omega_z}, \qquad (32)$$

and

$$\gamma = \frac{F_0 \alpha_l}{2\sqrt{\Omega}} \left(\frac{f_+}{\omega_1 - \omega_z} + \frac{f_-}{\omega_2 + \omega_z} \right). \qquad (33)$$

The Hamiltonian (30) is equivalent to that of a two-level Rabi problem with oscillations in occupation probabilities given by

$$P_1(t) = P_{\max} \sin^2(\omega_R t), \quad P_0(t) = 1 - P_1(t), \qquad (34)$$

where the amplitude, Rabi frequency, and the level separation are given by

$$P_{\max} = \frac{\gamma^2}{\hbar^2 \omega_R^2}, \qquad (35)$$

$$\omega_R = \left[\frac{\gamma^2}{\hbar^2} + \frac{(\omega - \omega_{21})^2}{4} \right]^{1/2}, \qquad (36)$$

and

$$\omega_{21} = \frac{E_2 - E_1}{\hbar} = \omega_z + \frac{\alpha_l^2 m}{\hbar} \left(\frac{f_-^2}{\omega_2 + \omega_z} - \frac{f_+^2}{\omega_1 - \omega_z} \right), \qquad (37)$$

respectively. Hence, the new resonance condition is $\omega = \omega_{21}$ due to the energy correction second order in α_l. The resonant Rabi frequency is $\omega_{\text{res}} = 2\gamma/\hbar$ and is hence, linearly proportional to both α_l and F_0.

At resonance, the time-evolved state is given by

$$|\psi(t)\rangle = \begin{pmatrix} e^{-iE_1 t/\hbar} \cos(\gamma \, t/\hbar) \\ e^{-iE_2 t/\hbar} \sin(\gamma \, t/\hbar) \end{pmatrix}. \qquad (38)$$

The expectation value of the spin vector follows the following trajectory:

$$\langle \boldsymbol{\sigma}(t)\rangle = [\cos\omega t \sin(2\gamma t/\hbar), -\sin\omega t \sin(2\gamma t/\hbar),$$
$$\times \cos(2\gamma t/\hbar)]. \qquad (39)$$

The Bloch sphere dynamics through a half Rabi cycle ($T_\pi = \pi/\omega_{\text{res}}$) is shown in Fig. 2 when the system is initialized in spin-up state. The spirals occur due to the finite $\langle\sigma_x(t)\rangle$ and $\langle\sigma_y(t)\rangle$ which oscillate with a frequency of ω. It can be shown that the number of rotations about the z axis is $\omega/(2\omega_{\text{res}})$. Since $\omega \gg \omega_{\text{res}}$ in our case, the spin vector $\langle\boldsymbol{\sigma}(t)\rangle$ makes a large number of rotations/precessions $\sim$2710 about the z axis before flipping down completely at $T = \pi/\omega_{\text{res}}$. Hence, the Rabi oscillation is not simply a "rotation" of the spin about x or y axis, but a spiralling-down motion. The irradiation by laser for half Rabi cycle acts as a π pulse with possible applications in designing a quantum NOT gate.

C. Numerical formalism

1. Unitary transformation

We know that the TDSE for a simple two-level system under circular driving can be solved exactly by purging the time-dependence of the Hamiltonian through an appropriate
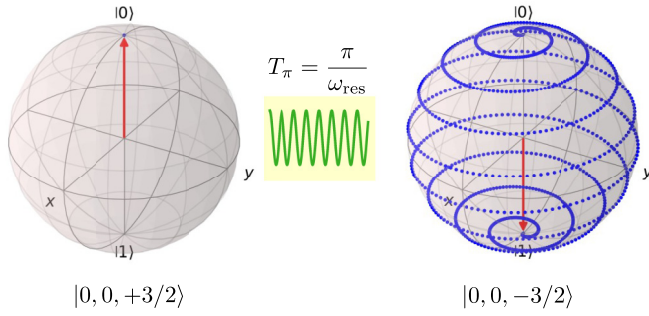
FIG. 2. Bloch sphere dynamics of the qubit on application of the laser beam for half Rabi cycle, i.e., $T_\pi = \pi/\omega_{res}$. We use the following system parameters: $\tilde{F}_0 = 0.02 \times 300$, $B = 0.5$ T, $\tilde{\alpha}_l = 0.0047$, $\tilde{\omega}_c = 0.303$, $\tilde{\omega}_z = 0.214$, $\omega = \omega_{21}$ which are defined in Sec. V. The spin-up state spirals down to the spin-down state on the Bloch sphere because the driving frequency is much larger than the Rabi frequency. Here, $\tilde{F}_0$ has been magnified 300 times the actual value for better visualization of the rotations (although a stronger drive leads to other effects which is discussed later). As a result, the spin vector rotates ~9 times about the z axis during the process of spin-flip.

unitary transformation. Using a similar approach and the fact that $[J_z^{(L)}, H_{FD} + H_R^{(L)}] = 0$ and $[J_z^{(C)}, H_{FD} + H_R^{(C)}] = 0$, we can deduce a static Hamiltonian $\mathcal{H}^{(L)}$ or $\mathcal{H}^{(C)}$ when either of the two Rashba couplings (linear or cubic) is present in the system (see Appendix C for details). For the velocity gauge, we deduce

$$\mathcal{H}^{(L)/(C)} = \mathcal{H}_0 + \mathcal{H}_R^{(L)/(C)}, \tag{40}$$

where

$$\mathcal{H}_0 = \hbar\Omega(\hat{n}_1 + \hat{n}_2 + 1) + \hbar\left(\omega - \frac{\omega_c}{2}\right)(\hat{n}_2 - \hat{n}_1)$$
$$+ \frac{|e|^2 A_0^2}{2m} - \frac{i|e|A_0\sqrt{m\hbar}}{2m}(f_+(\hat{a}_1^\dagger - \hat{a}_1) - f_-(\hat{a}_2^\dagger - \hat{a}_2)), \tag{41}$$

$$\mathcal{H}_R^{(L)} = \frac{\hbar}{2}(\omega - \omega_z)\sigma_z$$
$$+ \alpha_l[(\sqrt{m\hbar}(f_+\hat{a}_1^\dagger + f_-\hat{a}_2) + i|e|A_0)\sigma_+ + \text{H.c.}], \tag{42}$$

$$\mathcal{H}_R^{(C)} = \frac{\hbar}{2}(3\omega - \omega_z)\sigma_z$$
$$+ \alpha_c[(\sqrt{m\hbar}(f_+\hat{a}_1^\dagger + f_-\hat{a}_2) + i|e|A_0)^3\sigma_+ + \text{H.c.}]. \tag{43}$$

Similarly, for the length gauge, we get

$$\mathcal{H}'^{(L)/(C)} = \mathcal{H}_0' + \mathcal{H}_R'^{(L)/(C)}, \tag{44}$$

where

$$\mathcal{H}_0' = \hbar\Omega(\hat{n}_1 + \hat{n}_2 + 1) + \hbar\left(\omega - \frac{\omega_c}{2}\right)(\hat{n}_2 - \hat{n}_1)$$
$$+ \frac{iF_0}{2}\sqrt{\frac{\hbar}{m\Omega}}(\hat{a}_1 - \hat{a}_1^\dagger - \hat{a}_2 + \hat{a}_2^\dagger), \tag{45}$$

$$\mathcal{H}_R'^{(L)} = \frac{\hbar}{2}(\omega - \omega_z)\sigma_z + H_R^{(L)}, \tag{46}$$

$$\mathcal{H}_R'^{(C)} = \frac{\hbar}{2}(3\omega - \omega_z)\sigma_z + H_R^{(C)}, \tag{47}$$

and $H_R^{(C)}$ and $H_R^{(L)}$ are defined in Eqs. (11) and (12), respectively.

In this gauge, the time evolution operator of the system can be written as the ordered product of two unitary operators,

$$U'^{(L)/(C)}(t) = e^{i\hat{J}_z^{(L)/(C)}\omega t/\hbar} e^{-i\mathcal{H}'^{(L)/(C)}t/\hbar}. \tag{48}$$

The first factor accounts for the unitary transformation and the second, containing the static Hamiltonian, gives the dynamical phase in the transformed frame. For the velocity gauge, $\mathcal{H}'^{(L)/(C)}$ is simply replaced by $\mathcal{H}^{(L)/(C)}$ in the second exponential. If the system is initialized in a FD state $|n_1^i, n_2^i, s^i\rangle$, then the transition amplitude to a state $|n_1^f, n_2^f, s^f\rangle$ is

$$a_f(t) = e^{i(n_2^f - n_1^f + s^{f(L)/(C)})\omega t}$$
$$\times \sum_m e^{-i\varepsilon_m' t/\hbar}\langle n_1^f, n_2^f, s^f|\varepsilon_m'\rangle\langle\varepsilon_m'|n_1^i, n_2^i, s^i\rangle, \tag{49}$$

where $\mathcal{H}'^{(L)/(C)}|\varepsilon_m'\rangle = \varepsilon_m'|\varepsilon_m'\rangle$, $s^{f(L)} = s^f/3$, and $s^{f(C)} = s^f$, with $s^f = \pm 3/2$. The eigenvectors of $\mathcal{H}'^{(L)/(C)}$ can be obtained numerically by truncating its matrix up to a sufficiently large number of FD levels. With $|0, 0, 3/2\rangle$ as the initial state, we then obtain the occupation probabilities of the states $|0, 0, \pm 3/2\rangle$ as a function of time by computing $|a_f(t)|^2$ using Eq. (49).

2. Floquet theory

When both the Rashba couplings are present, we do not have a suitable unitary transformation to make the Hamiltonian time-independent. On periodic driving, the basis of Floquet states is more relevant to work with as they behave like static states in an extended Hilbert space of the driven system. They evolve similar to the static energy eigenstates but with a sum of quasienergy values and "n" multiples of photon energies contained in their dynamical phases. Since the Hamiltonian of the driven dot is periodic in time, the dynamics can be studied using Floquet theory. By Floquet's theorem, the following solutions to the TDSE exist:

$$|u(t)\rangle = e^{-i\epsilon_\eta t/\hbar}|\phi_\eta(t)\rangle, \tag{50}$$

where ϵ_η are the real-valued quasienergies and $|\phi_\eta(t)\rangle$ are the corresponding Floquet modes periodic in time. Considering the FD states as $|n_1, n_2, s\rangle \equiv |l\rangle$, the transition amplitude ($i \to f$) can be written as (see Appendices D and E for detailed derivation),

$$a_f(t) = \sum_\eta \left(\sum_{n'}(c_{i,\eta}^{n'})^*\right)\left(\sum_n c_{f,\eta}^n e^{-i(\epsilon_\eta - n\hbar\omega)t/\hbar}\right), \tag{51}$$

where l_{max} is the maximum number of FD levels considered in the problem and $c_{l,\eta}^n$ is defined in Eq. (D6). The number of independent Floquet modes is equal to the number of FD levels considered in the calculation. The Floquet modes can be
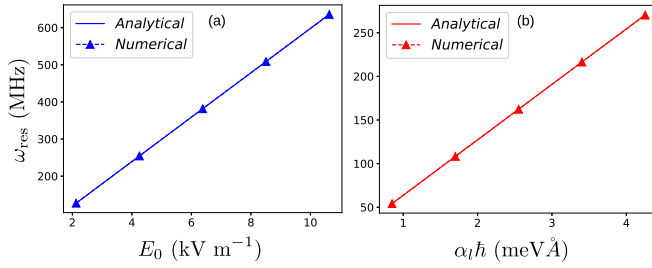
FIG. 3. Comparison between analytical and numerical values of resonant Rabi frequencies. (a) Variation of ω_{res} with the radiation amplitude E_0 for $\alpha_l = 2.01$ meV Å/$\hbar$ and $B = 0.5$ T. (b) Variation of ω_{res} with α_l for $E_0 = 2.172$ kV/m and $B = 0.5$ T.

obtained by numerical diagonalization of the Floquet Hamiltonian truncated up to a large number of FD levels and the occupation probabilities $|a_f(t)|^2$ of the states $|0, 0, \pm 3/2\rangle$ can hence be calculated using Eq. (51).

V. RESULTS AND DISCUSSION

Let us define dimensionless quantities as $\tilde{\omega}_z = \omega_z/\omega_0$, $\tilde{\omega}_c = \omega_c/\omega_0$, $\tilde{\omega} = \omega/\omega_0$, $\tilde{\alpha}_c = \alpha_c p_0^3/(\hbar\omega_0)$, $\tilde{\alpha}_l = \alpha_l p_0/(\hbar\omega_0)$ and $\tilde{F}_0 = F_0/(p_0\omega_0)$ where $p_0 = \sqrt{\hbar m \omega_0}$. For a confinement length $l_0 = 20$ nm and using known values of parameters for Ge/Si quantum wells [57,62,75], i.e., $m \sim 0.09 \, m_e$, $g_\perp \approx 15.7$, $\alpha_c = 2.26 \times 10^5$ meV Å^3/$\hbar^3$, $\alpha_l = 2.01$ meV Å/$\hbar$, we get $\tilde{\alpha}_l = 0.0047$, $\tilde{\omega}_z = 0.428\,B$, and $\tilde{\omega}_c = 0.606\,B$, where B is the magnetic field strength in Tesla. For all the results that follow, we use these parameters unless stated otherwise. For $B = 0.5$ T, the resonant driving frequency is $\omega \approx \omega_z = 6.9 \times 10^{11}$ Hz. For $\tilde{F}_0 = 0.02$, $E_0 \approx 2127$ V/m which is well within the attainable limits for modern-day lasers.

A. Analytical results

For $\tilde{F}_0 = 0.02$ and $B = 0.5$ T and the system parameters mentioned above, we get $\omega_{res} = 127.24$ MHz. This value can be increased further by applying stronger laser beams. Figure 3 shows excellent agreement between the analytically and numerically computed values of resonant Rabi frequencies for small values of $\tilde{\alpha}_l$ and $\tilde{F}_0$. Figure 4 shows density plots of the probability amplitude $P_{\max}$ from Eq. (35) as a function of $\tilde{\omega}$ and $\tilde{\alpha}_l$ for a fixed radiation amplitude $\tilde{F}_0 = 0.08$ and different values of magnetic field: (a) $B = 0.5$ T, (b) $B = 1.0$ T, and (c) $B = 1.5$ T. The dark curves on the plots indicate the resonances in $P_{\max}$. The width of the resonances ($\propto \gamma$) gradually increases with B and α_l. Since the linear Rashba strength is nearly fixed by the calculations [57,62], sharper resonances can be achieved by working at low magnetic fields.

B. Numerical results

First, we use the method of unitary transformation to obtain the Rabi oscillations when $\alpha_l \neq 0$, $\alpha_c = 0$. Figure 5 shows variation of occupation probabilities of the ground ($|0, 0, 3/2\rangle$) and first excited ($|0, 0, -3/2\rangle$) states of the dot, labeled as $P_0(t)$ and $P_1(t)$, respectively, with time for different values of radiation amplitude when the system is initialized in the ground state and the resonance condition is satisfied. The
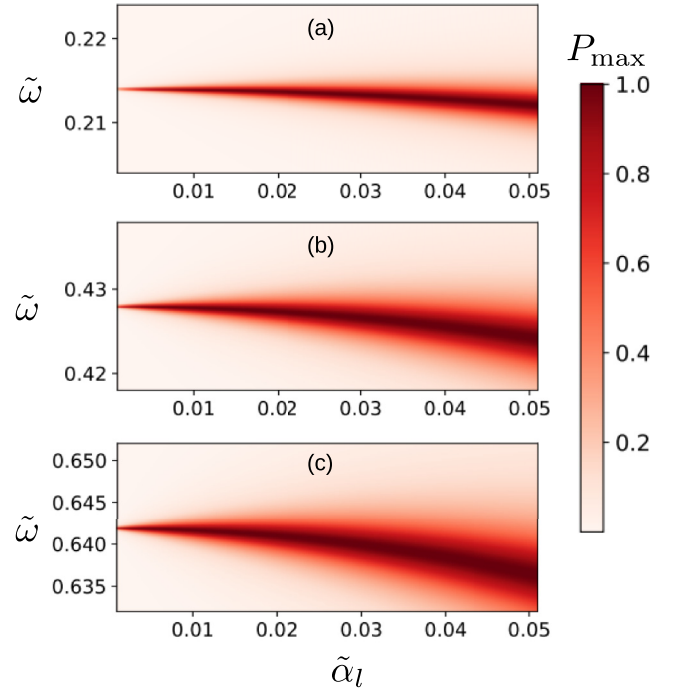

FIG. 4. Plot of maximum transition probability as a function of $\tilde{\omega}$ and $\tilde{\alpha}_l$ for a fixed radiation amplitude $\tilde{F}_0 = 0.08$ and different values of magnetic field: (a) $B = 0.5$ T, (b) $B = 1.0$ T, and (c) $B = 1.5$ T. The dark curves indicate the resonances. The width of the resonances increase with B and α_l.

resonant Rabi frequency clearly increases with the radiation amplitude, as expected from the expression of ω_{res}. Similar behavior is displayed with respect to the variation of α_l. The numerical methods can also be used to study the time evolution of the qubit for stronger electrical drives characterized by larger values of $\tilde{F}_0$. This would incorporate the higher
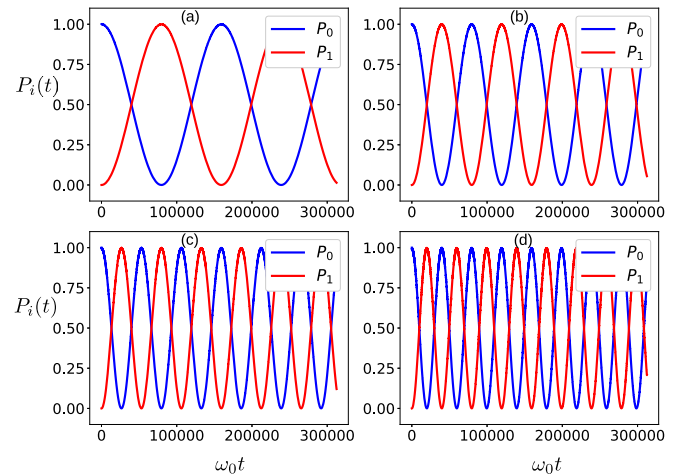

FIG. 5. Plots of occupation probability as a function of time for realistic system parameters (i.e., $B = 0.5$ T, $\tilde{\alpha}_l = 0.0047$, $\tilde{\omega}_c = 0.303$, $\tilde{\omega}_z = 0.214$, $\omega = \omega_{21}$) and different values of driving strength: (a) $\tilde{F}_0 = 0.02$, (b) $\tilde{F}_0 = 0.04$, (c) $\tilde{F}_0 = 0.06$, and (d) $\tilde{F}_0 = 0.08$. The resonant Rabi frequency is an increasing function of the driving strength.
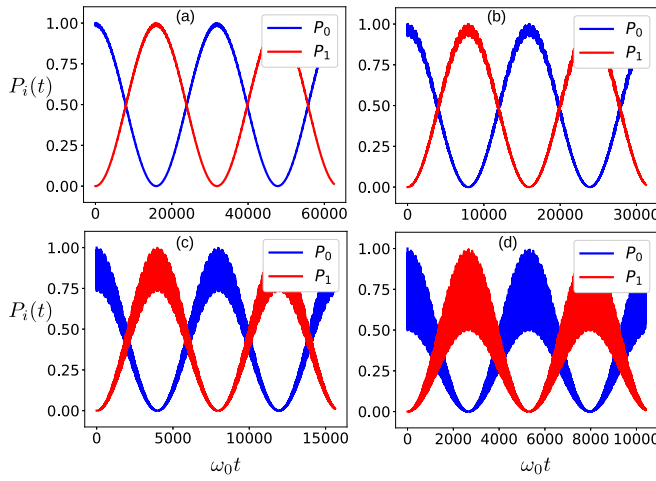
FIG. 6. Plots of occupation probability as a function of time for realistic system parameters (i.e., $B = 0.5$ T, $\tilde{\alpha}_l = 0.0047$, $\tilde{\omega}_c = 0.303$, $\tilde{\omega}_z = 0.214$, $\omega = \omega_{21}$) and larger values of radiation amplitude: (a) $\tilde{F}_0 = 0.1$, (b) $\tilde{F}_0 = 0.2$, (c) $\tilde{F}_0 = 0.4$, and (d) $\tilde{F}_0 = 0.6$.

order terms of the perturbation theory discussed in Sec. IV B. Figure 6 shows the probability oscillations for stronger laser beams. We observe that the resonant Rabi frequency increases but a high-frequency noise, whose amplitude grows with F_0, is superimposed on the Rabi oscillations. Its origin can be explained using the results of the Schrieffer-Wolff transformation. On the right-hand side of Eq. (B8), H_{SW}^0 represents the undriven diagonal (up to the order of α_l^2) Hamiltonian, $V_g(t)$ couples identical spin states with identical orbital quantum numbers and $[S, V_g(t)]$ couples opposite spin states with same orbital quantum number. For low driving strengths, effect of $V_g(t)$ is negligible as compared to $[S, V_g(t)]$ and nearly no transitions take place from the ground state to the excited states with higher orbital quantum numbers. For larger driving strengths, $V_g(t)$ competes with $[S, V_g(t)]$ and off-resonant transitions ($|\Delta n_i| \neq 0$) with smaller amplitudes but a much larger frequency than the resonant ($n_1 = n_2 = 0$, $\Delta s = \pm 3$,) oscillations take place in addition to the latter. Those transitions appear as a high-frequency noise overlapped with the original Rabi oscillations since the total probability has to be conserved. This noise would hamper the fidelity of the quantum gate at the cost of faster operations. Hence, a low laser amplitude ($\sim$2–8 kV/m) is recommendable to perform qubit rotations in this system with a good accuracy. The inefficiency of EDSR for stronger drives has also been observed in double quantum dots [28].

As mentioned earlier, no probability oscillations are observed for $\alpha_l = 0$, $\alpha_c \neq 0$ as the cubic Rashba coupling does not support EDSR. When both $\alpha_l \neq 0$ and $\alpha_c \neq 0$, the method of unitary transformation fails and hence we use Floquet theory to obtain the time dynamics. First, we elaborate how the Floquet theory explains the time evolution. In Eq. (51), the term within the first parenthesis represents the projection of the initial state on the ηth Floquet mode. The different nth-order sidebands of the ηth Floquet mode evolve in time with dynamical phases $e^{-i(\epsilon_\eta - n\hbar\omega)t/\hbar}$. The term within the second parenthesis denotes the dynamical transition amplitudes from the ηth Floquet mode with "$-n$" photons (or nth order

sideband) to the lth FD level. For a strictly two-level Rabi problem at resonance, the ground and first excited states have equal magnitudes of projections ($= 1/\sqrt{2}$) on each of the Floquet modes and also the first excited state has its projection on the sideband of same photon number n for each η. As a result, the final transition amplitude from $|0\rangle \to |1\rangle$ is a sum of two oscillating terms viz. $e^{-i(\epsilon_0 - n\hbar\omega)t/\hbar}$ and $e^{-i(\epsilon_1 - n\hbar\omega)t/\hbar}$ of equal magnitudes, which give rise to Rabi oscillations of frequency equal to the quasienergy difference only, i.e., $\omega_{res} = |\epsilon_0 - \epsilon_1|/\hbar$ and maximum transition probability equal to $2 \times (1/\sqrt{2})^2 = 1$.

Using Eq. (51), the transition probability to the lth FD state can be simplified as

$$
P_l(t) = |a_l(t)|^2 = \sum_{\{\chi\}, \eta > \zeta, n > m}
$$

$$
\times 2R_{lmnm'n'}^{\eta\zeta} \cos\left[\frac{(\Delta\epsilon_{\eta\zeta} - \Delta_{nm}\hbar\omega)t}{\hbar} + \theta_{lmnm'n'}^{\eta\zeta}\right]
$$

$$
+ \sum_{\{\kappa\}, \eta > \zeta} 2R_{lnnm'n'}^{\eta\zeta} \cos\left[\Delta\epsilon_{\eta\zeta}t/\hbar + \theta_{lnnm'n'}^{\eta\zeta}\right]
$$

$$
+ \sum_{\{\rho\}, n > m} 2R_{lmnm'n'}^{\eta\eta} \cos\left[-\Delta_{nm}\omega t + \theta_{lmnm'n'}^{\eta\eta}\right]
$$

$$
+ \sum_{\{\xi\}} |c_{l\eta}^n|^2 (c_{0,\eta}^{n'})^* (c_{0,\eta}^{m'}), \tag{52}
$$

where $\{\chi\} = \{\eta, n, n', \zeta, m, m'\}$, $\{\kappa\} = \{\eta, n, n', \zeta, m'\}$, $\{\rho\} = \{\eta, n, n', m, m'\}$, $\{\xi\} = \{\eta, n, n', m'\}$, $\Delta\epsilon_{\eta\zeta} = \epsilon_\eta - \epsilon_\zeta$, $\Delta_{nm} = n - m$, $R_{lmnm'n'}^{\eta\zeta} = |c_{l,\eta}^n (c_{0,\eta}^{n'})^* (c_{l,\zeta}^m)^* c_{0,\zeta}^{m'}|$, and $\theta_{lmnm'n'}^{\eta\zeta} = \text{Arg}[c_{l,\eta}^n (c_{0,\eta}^{n'})^* (c_{l,\zeta}^m)^* c_{0,\zeta}^{m'}]$.
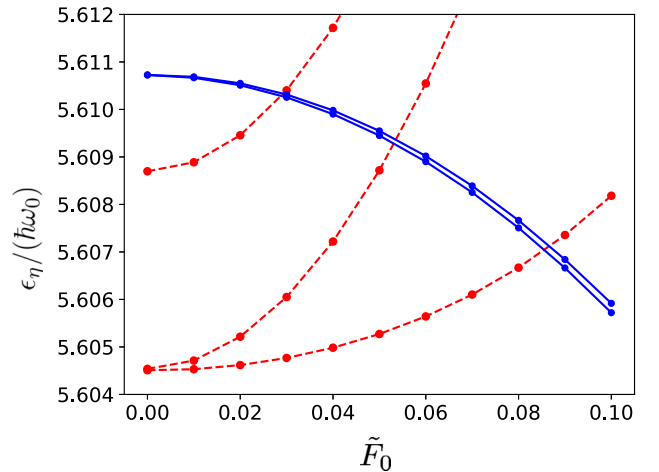

FIG. 7. Variation of quasienergies of certain Floquet levels with radiation amplitude for realistic system parameters (i.e., $B = 0.5$ T, $\tilde{\alpha}_l = 0.0047$, $\tilde{\omega}_c = 0.303$, $\tilde{\omega}_z = 0.214$, $\omega = \omega_{21}$). The quasienergies of the levels represented by the red dotted curves decrease with F_0 and also do not contribute to the Rabi oscillations for the given initial and final states. The levels represented by the blue solid curves participate in the Rabi rotations and the Rabi frequency, equal to the gap between them, increases (linearly) with F_0.
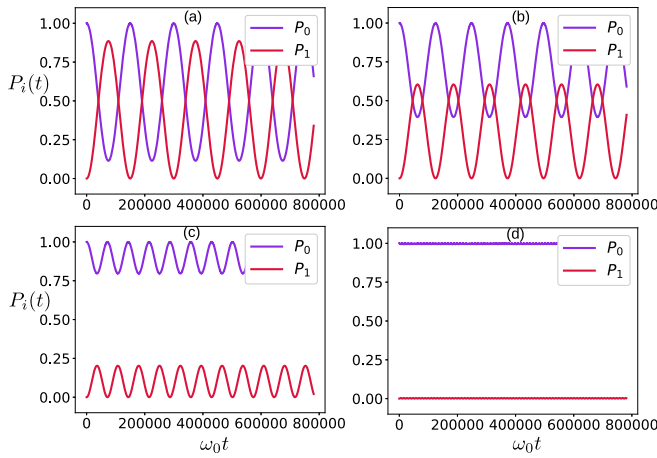
FIG. 8. Plots of occupation probability as a function of time for realistic system parameters (i.e., $B = 0.5$ T, $\tilde{\alpha}_l = 0.0047$, $\tilde{\omega}_c = 0.303$, $\tilde{\omega}_z = 0.214$, $\tilde{F}_0 = 0.02$, $\omega = \omega_{21}$) and different values of cubic Rashba coupling: (a) $\tilde{\alpha}_c = 0.002$, (b) $\tilde{\alpha}_c = 0.003$, (c) $\tilde{\alpha}_c = 0.0047$ (equal to α_l), and (d) $\tilde{\alpha}_c = 0.013$ (typical value). The Rabi oscillations become increasingly nonresonant with increase in α_c and nearly vanish for typical values for α_c for this system.

For the multilevel system in consideration, we find that the second summation in Eq. (52) is the dominant contribution to the time-dependent part of the oscillations. This means that two quasienergy levels with an identical photon number contribute to the Rabi oscillations. Figure 7 shows the variation of quasienergies of some of the Floquet levels with the radiation amplitude at resonance and in absence of cubic Rashba coupling. The levels denoted by the blue curves are the ones which have equal projections on both the initial ($|0, 0, +3/2\rangle$) and final ($|0, 0, -3/2\rangle$) FD levels. Hence, these are the levels which participate in the Rabi oscillations in Floquet picture and the Rabi frequency is equal to the difference of their quasienergies. The gap between the levels increases (linearly) with the radiation amplitude and is consistent with the values of ω_{res}.

In Fig. 8, we study the dependence of the resonant Rabi oscillations on the cubic Rashba strength α_c using numerical results of the Floquet theory. We observe a gradual diminishing of the resonant Rabi oscillations on increasing the values of α_c. We find that that oscillations nearly disappear for realistic values of α_c.

VI. CONCLUSION

To conclude, we have studied the time dynamics of a planar Ge hole spin-qubit driven by coherent circularly polarized radiation in the presence of an out-of-plane magnetic field and Rashba SOCs. The coherent beam may be supplied by ultrafast laser pulses which have been extensively used in recent years for Floquet engineering. We consider the recently claimed p-linear and the dominant spherically symmetric component of the p-cubic Rashba SOC found in heavy holes. We show that a laser drive of suitable frequency can be used to perform qubit rotations in the presence of linear Rashba

coupling (only), an effect similar to EDSR with ac gate-voltages. We have shown how the problem can be solved using two different gauges viz. velocity and length gauges. For small Rashba strength and weak laser beam, we use perturbation theory and make a Schrieffer-Wolff transformation to obtain an analytical form of the Rabi frequency. The Rabi frequency is linearly proportional to the radiation amplitude and the linear Rashba strength. For a laser beam of electric field amplitude 2.127 kV/m, the Rabi frequency is approximately 127 MHz for realistic system parameters. We observe that the width of resonance increases with increase in strengths of the magnetic field and Rashba coupling.

For higher radiation amplitude, we employ methods of unitary transformation and Floquet theory independently for numerical computation of the qubit dynamics. The method of unitary transformation deals with transforming to a rotating frame of reference and exploiting the rotational symmetry of the system in the total Hilbert space of spin and orbital degrees of freedom. This method is valid when only one of the two Rashba couplings (linear or cubic) is present. Hence, we use it to study the effect of stronger laser beams in the Rabi oscillations when only linear Rashba coupling is considered. We encounter a high-frequency noise in the Rabi oscillations for stronger laser beams thereby rendering the drive unsuitable for qubit manipulation. As already known, no Rabi oscillations occur when only cubic Rashba coupling is present in the system.

We have used Floquet theory to solve the Schrödinger equation when both linear and cubic Rashba couplings are simultaneously present in the system. The numerical results show that the Rabi oscillations gradually diminish as we increase the cubic Rashba strength for a fixed linear Rashba paramater. This implies that the system is driven out of resonance by the cubic Rashba coupling. For a realistic value of the cubic Rashba parameter, the Rabi oscillations nearly vanish despite the presence of linear Rashba coupling. Hence, the cubic Rashba coupling, which can be controlled by changing the interfcial electric field using gate electrodes, has to be highly minimized to observe resonant Rabi oscillations in this system. We have also shown that the Rabi frequency is equal to the quasienergy gap between two Floquet levels which is an increasing function of radiation amplitude.

Our results may be useful to achieve optical control of hole qubits in Ge quantum dots. With photolithography already boosting the semiconductor fabrication industry, the use of coherent laser beams for manipulation of spin-qubits is another attractive option to develop quantum NOT gates with the aid of strong SOC of the heavy-hole states in 2D Ge heterostructures.

APPENDIX A: MATRIX ELEMENTS OF H_R AND V_n

The matrix elements of H_R in the FD basis are

$$\langle n_1', n_2', s'|H_R|n_1, n_2, s\rangle = f_0(n_1', n_2', n_1, n_2)\delta_{s',3/2}\,\delta_{s,-3/2} + f_0(n_1, n_2, n_1', n_2')\delta_{s',-3/2}\,\delta_{s,3/2}, \tag{A1}$$

where

$$
\begin{aligned}
f_0(n_1', n_2', n_1, n_2) &= \alpha_c(m\hbar)^{3/2}\big[f_-^3\sqrt{n_2(n_2-1)(n_2-2)}\,\delta_{n_1',n_1}\,\delta_{n_2',n_2-3} + 3f_-^2 f_+\sqrt{(n_1+1)n_2(n_2-1)}\,\delta_{n_1',n_1+1}\,\delta_{n_2',n_2-2} \\
&\quad + 3f_- f_+^2\sqrt{(n_1+1)(n_1+2)n_2}\,\delta_{n_1',n_1+2}\,\delta_{n_2',n_2-1} + f_+^3\sqrt{(n_1+1)(n_1+2)(n_1+3)}\,\delta_{n_1',n_1+3}\,\delta_{n_2',n_2}\big] \\
&\quad + \alpha_l\sqrt{m\hbar}\big[f_+\sqrt{n_1+1}\,\delta_{n_1',n_1+1}\,\delta_{n_2',n_2} + f_-\sqrt{n_2}\,\delta_{n_1',n_1}\,\delta_{n_2',n_2-1}\big].
\end{aligned}
\tag{A2}
$$

The matrix elements of V_n are

$$\langle n_1', n_2', s'|V_0|n_1, n_2, s\rangle = \frac{|e|^2 A_0^2}{2m}\,\delta_{n_1',n_1}\,\delta_{n_2',n_2}\,\delta_{s',s}, \tag{A3}$$

$$
\begin{aligned}
\langle n_1', n_2', s'|V_1|n_1, n_2, s\rangle &= 3i\alpha_c|e|A_0 m\hbar\big[f_+^2\sqrt{(n_1+1)(n_1+2)}\,\delta_{n_1',n_1+2}\,\delta_{n_2',n_2} + 2f_+ f_-\sqrt{(n_1+1)n_2}\,\delta_{n_1',n_1+1}\,\delta_{n_2',n_2-1} \\
&\quad + f_-^2\sqrt{n_2(n_2-1)}\,\delta_{n_1',n_1}\,\delta_{n_2',n_2-2}\big]\delta_{s',3/2}\,\delta_{s,-3/2} \;+\; i\alpha_l|e|A_0\,\delta_{n_1',n_1}\,\delta_{n_2',n_2}\,\delta_{s',3/2}\,\delta_{s,-3/2} \\
&\quad \times i\frac{|e|A_0}{2m}\sqrt{m\hbar}\big[f_+\sqrt{n_1}\,\delta_{n_1',n_1-1}\,\delta_{n_2',n_2} + f_-\sqrt{n_2+1}\,\delta_{n_1',n_1}\,\delta_{n_2',n_2+1}\big]\delta_{s',s},
\end{aligned}
\tag{A4}
$$

$$\langle n_1', n_2', s'|V_2|n_1, n_2, s\rangle = -3\alpha_c\sqrt{m\hbar}|e|^2 A_0^2\big[f_+\sqrt{n_1+1}\,\delta_{n_1',n_1+1}\,\delta_{n_2',n_2} + f_-\sqrt{n_2}\,\delta_{n_1',n_1}\,\delta_{n_2',n_2-1}\big]\delta_{s',3/2}\,\delta_{s,-3/2}, \tag{A5}$$

and

$$\langle n_1', n_2', s'|V_3|n_1, n_2, s\rangle = -i\alpha_c|e|^3 A_0^3\,\delta_{n_1',n_1}\,\delta_{n_2',n_2}\,\delta_{s',3/2}\,\delta_{s,-3/2}. \tag{A6}$$

APPENDIX B: SCHRIEFFER-WOLFF TRANSFORMATION

The SW transformation can be written as

$$H_{\mathrm{SW}}^0 = e^S(H_{\mathrm{FD}} + H_R)e^{-S} \approx H_{\mathrm{FD}} + [S, H_R]/2, \tag{B1}$$

where $S^\dagger = -S$ and

$$[H_{\mathrm{FD}}, S] = H_R. \tag{B2}$$

We consider the following ansatz for S:

$$S = \hat{S}^{(1)} + \hat{S}^{(2)}\sigma_+ - \hat{S}^{(2)\dagger}\sigma_-, \tag{B3}$$

where $\hat{S}^{(i)} = S_{1a}^{(i)}\hat{a}_1 + S_{1b}^{(i)}\hat{a}_1^\dagger + S_{2a}^{(i)}\hat{a}_2 + S_{2b}^{(i)}\hat{a}_2^\dagger$ with $i = 1, 2$. Using Eqs. (B3) in (B2) and comparing both the sides, we get $\hat{S}^{(1)} = 0$ and

$$\hat{S}^{(2)} = \alpha\sqrt{\frac{m}{\hbar}}\left(\frac{f_+}{\omega_1 - \omega_z}\hat{a}_1^\dagger - \frac{f_-}{\omega_2 + \omega_z}\hat{a}_2\right). \tag{B4}$$

Using Eq. (B4) in Eq. (B1), we get

$$H_{SW}^0 = H_{\mathrm{FD}} + \hat{\xi}_+\mathbb{P}_+ + \hat{\xi}_-\mathbb{P}_-, \tag{B5}$$

where $\mathbb{P}_\pm = (1 \pm \sigma_z)/2$ are the spin-projection operators and

$$
\begin{aligned}
\hat{\xi}_+ = \frac{\alpha_l^2 m}{2}\bigg[&\frac{2f_+^2}{\omega_1 - \omega_z}\hat{n}_1 - \frac{2f_-^2}{\omega_2 + \omega_z}(1 + \hat{n}_2) \\
&+ f_+ f_-(\hat{a}_1\hat{a}_2 + \hat{a}_2^\dagger\hat{a}_1^\dagger)\left(\frac{1}{\omega_1 - \omega_z} - \frac{1}{\omega_2 + \omega_z}\right)\bigg],
\end{aligned}
\tag{B6}
$$

$$
\begin{aligned}
\hat{\xi}_- = -\frac{\alpha_l^2 m}{2}\bigg[&\frac{2f_+^2}{\omega_1 - \omega_z}(1 + \hat{n}_1) - \frac{2f_-^2}{\omega_2 + \omega_z}\hat{n}_2 \\
&+ f_+ f_-(\hat{a}_1\hat{a}_2 + \hat{a}_2^\dagger\hat{a}_1^\dagger)\left(\frac{1}{\omega_1 - \omega_z} - \frac{1}{\omega_2 + \omega_z}\right)\bigg].
\end{aligned}
\tag{B7}
$$

For a weak driving ($\frac{F_0}{\hbar\omega_0}\sqrt{\frac{\hbar}{m\omega_0}} = \tilde{F}_0 \ll 1$), the SW Hamiltonian can be written as

$$
\begin{aligned}
H_{\mathrm{SW}}(t) &= H_{\mathrm{SW}}^0 + e^S V_g(t)e^{-S} \\
&\approx H_{\mathrm{SW}}^0 + V_g(t) + [S, V_g(t)].
\end{aligned}
\tag{B8}
$$

Then, the lowest energy block of $H_{\mathrm{SW}}(t)$ (spanned by $|0, 0, \pm 3/2\rangle$ states) can be written as

$$
\begin{aligned}
H_{\mathrm{eff}}(t) &= -\frac{\hbar\omega_z}{2}\sigma_z - \frac{\alpha_l^2 m f_-^2}{\omega_2 + \omega_z}\mathbb{P}_+ - \frac{\alpha_l^2 m f_+^2}{\omega_1 - \omega_z}\mathbb{P}_- \\
&\quad - i\gamma e^{i\omega t}\sigma_+ + i\gamma e^{-i\omega t}\sigma_- \\
&= \begin{pmatrix} -\frac{\hbar\omega_z}{2} - \frac{\alpha_l^2 m f_-^2}{\omega_2 + \omega_z} & -i\gamma e^{i\omega t} \\ i\gamma e^{-i\omega t} & \frac{\hbar\omega_z}{2} - \frac{\alpha_l^2 m f_+^2}{\omega_1 - \omega_z} \end{pmatrix},
\end{aligned}
\tag{B9}
$$

where

$$\gamma = \frac{F_0\alpha_l}{2\sqrt{\Omega}}\left(\frac{f_+}{\omega_1 - \omega_z} + \frac{f_-}{\omega_2 + \omega_z}\right). \tag{B10}$$

APPENDIX C: METHOD OF UNITARY TRANSFORMATION

We can get a static Hamiltonian through a unitary transformation when at least one of the Rashba couplings is absent. Imposing this condition, the driven Hamiltonian in the velocity gauge containing exclusively the linear or cubic Rashba coupling is given by

$$H^{(\mathrm{L})/(\mathrm{C})}(t) = H_{\mathrm{FD}} + H_r(t) + H_R^{(\mathrm{L})/(\mathrm{C})}(t), \tag{C1}$$

where

$$H_r(t) = \frac{|e|^2 A_0^2}{2m} - \frac{|e|A_0}{m}(P_x \cos \omega t - P_y \sin \omega t), \quad \text{(C2)}$$

$$H_R^{(\text{L})}(t) = \alpha_l[-i(P_- - |e|A_0 e^{i\omega t})\sigma_+ + \text{H.c.}], \quad \text{(C3)}$$

and

$$H_R^{(\text{C})}(t) = \alpha_c[i(P_- - |e|A_0 e^{i\omega t})^3 \sigma_+ + \text{H.c.}]. \quad \text{(C4)}$$

In the length gauge, the driven Hamiltonian is simply

$$H'^{(\text{L})/(\text{C})}(t) = H_{\text{FD}} + H_R^{(\text{L})/(\text{C})} + V_g(t). \quad \text{(C5)}$$

The driven Hamiltonians in either gauge can be reduced to a static one by solving the TDSE in a frame rotating with $\mathbf{A}_r$. If $|\psi(t)\rangle$ is the solution in the rest frame, then the solution in the rotating frame, having angular speed "$-\omega$" (clockwise) about z axis, is given by

$$|\Phi(t)\rangle = \mathcal{R}_z(\omega t)|\psi(t)\rangle, \quad \text{(C6)}$$

where $\mathcal{R}_z$ is the standard rotation operator about z axis. For the driven Rashba Hamiltonian, it can be written as

$$\mathcal{R}_z^{(\text{L})/(\text{C})}(\omega t) = e^{-i\hat{J}_z^{(\text{L})/(\text{C})}\omega t/\hbar}, \quad \text{(C7)}$$

where $\hat{J}_z^{(\text{L})/(\text{C})}$ are defined in Eqs. (14) and (15). Using Eq. (C6) in the TDSE and working with the Hamiltonian in length gauge, we get

$$i\hbar \frac{\partial}{\partial t}|\Phi(t)\rangle = \left(\mathcal{R}_z H'^{(\text{L})/(\text{C})}(t)\mathcal{R}_z^\dagger + i\hbar \mathcal{R}_z^\dagger \frac{\partial}{\partial t}\mathcal{R}_z\right)|\Phi(t)\rangle. \quad \text{(C8)}$$

where $\mathcal{R}_z \equiv \mathcal{R}_z^{(\text{L})/(\text{C})}$. Using Eq. (C7), it reduces to

$$i\hbar \frac{\partial}{\partial t}|\Phi(t)\rangle = \mathcal{H}'^{(\text{L})/(\text{C})}|\Phi(t)\rangle, \quad \text{(C9)}$$

where

$$\mathcal{H}'^{(\text{L})/(\text{C})} = H'^{(\text{L})/(\text{C})}(t=0) + \hat{J}_z^{(\text{L})/(\text{C})}\omega \quad \text{(C10)}$$

is the time-independent Hamiltonian in the rotating frame. In terms of ladder operators, the transformed Hamiltonian in the velocity gauge can be written as

$$\mathcal{H}^{(\text{L})/(\text{C})} = \mathcal{H}_0 + \mathcal{H}_R^{(\text{L})/(\text{C})} \quad \text{(C11)}$$

where

$$\mathcal{H}_0 = \hbar\Omega(\hat{n}_1 + \hat{n}_2 + 1) + \hbar\left(\omega - \frac{\omega_c}{2}\right)(\hat{n}_2 - \hat{n}_1) + \frac{|e|^2 A_0^2}{2m}$$

$$- \frac{i|e|A_0\sqrt{m\hbar}}{2m}(f_+(\hat{a}_1^\dagger - \hat{a}_1) - f_-(\hat{a}_2^\dagger - \hat{a}_2)), \quad \text{(C12)}$$

$$\mathcal{H}_R^{(\text{L})} = \frac{\hbar}{2}(\omega - \omega_z)\sigma_z$$

$$+ \alpha_l[(\sqrt{m\hbar}(f_+\hat{a}_1^\dagger + f_-\hat{a}_2) + i|e|A_0)\sigma_+ + \text{H.c.}], \quad \text{(C13)}$$

$$\mathcal{H}_R^{(\text{C})} = \frac{\hbar}{2}(3\omega - \omega_z)\sigma_z$$

$$+ \alpha_c[(\sqrt{m\hbar}(f_+\hat{a}_1^\dagger + f_-\hat{a}_2) + i|e|A_0)^3\sigma_+ + \text{H.c.}]. \quad \text{(C14)}$$

Similarly, for the length gauge, we get

$$\mathcal{H}'^{(\text{L})/(\text{C})} = \mathcal{H}_0' + \mathcal{H}_R'^{(\text{L})/(\text{C})}, \quad \text{(C15)}$$

where

$$\mathcal{H}_0' = \hbar\Omega(\hat{n}_1 + \hat{n}_2 + 1) + \hbar\left(\omega - \frac{\omega_c}{2}\right)(\hat{n}_2 - \hat{n}_1)$$

$$+ \frac{iF_0}{2}\sqrt{\frac{\hbar}{m\Omega}}(\hat{a}_1 - \hat{a}_1^\dagger - \hat{a}_2 + \hat{a}_2^\dagger), \quad \text{(C16)}$$

$$\mathcal{H}_R'^{(\text{L})} = \frac{\hbar}{2}(\omega - \omega_z)\sigma_z + H_R^{(\text{L})}, \quad \text{(C17)}$$

$$\mathcal{H}_R'^{(\text{C})} = \frac{\hbar}{2}(3\omega - \omega_z)\sigma_z + H_R^{(\text{C})}, \quad \text{(C18)}$$

and $H_R^{(\text{C})}$ and $H_R^{(\text{L})}$ are defined in Eqs. (11) and (12), respectively.

Hence, the time-evolved state in the rest frame

$$|\psi(t)\rangle = \mathcal{R}_z^\dagger|\Phi(t)\rangle = e^{i\hat{J}_z^{(\text{L})/(\text{C})}\omega t/\hbar}e^{-i\mathcal{H}'^{(\text{L})/(\text{C})}t/\hbar}|\psi(0)\rangle. \quad \text{(C19)}$$

If the system is initialized in an FD state $|n_1^i, n_2^i, s^i\rangle$, then the transition amplitude to a state $|n_1^f, n_2^f, s^f\rangle$ is

$$a_f(t) = \langle n_1^f, n_2^f, s^f|\psi(t)\rangle$$

$$= e^{i(n_2^f - n_1^f + s^{f(\text{L})/(\text{C})})\omega t} \sum_m e^{-i\varepsilon_m' t/\hbar} d_{f,m}'(d_{i,m}')^*, \quad \text{(C20)}$$

where $\mathcal{H}'^{(\text{L})/(\text{C})}|\varepsilon_m'\rangle = \varepsilon_m'|\varepsilon_m'\rangle$, $d_{f,m}' = \langle n_1^f, n_2^f, s^f|\varepsilon_m'\rangle$, $d_{i,m}' = \langle n_1^i, n_2^i, s^i|\varepsilon_m'\rangle$, $s^{f(\text{L})} = s^f/3$, and $s^{f(\text{C})} = s^f$, with $s^f = \pm 3/2$. The transition probabilities are

$$P_f(t) = \sum_{m,n} e^{-i(\varepsilon_m' - \varepsilon_n')t/\hbar} d_{f,m}'(d_{i,m}')^*(d_{f,n}')^* d_{i,n}',$$

$$= \sum_m |d_{f,m}'|^2 |d_{i,m}'|^2$$

$$+ \sum_{m\neq n} e^{-i(\varepsilon_m' - \varepsilon_n')t/\hbar} d_{f,m}'(d_{i,m}')^*(d_{f,n}')^* d_{i,n}'. \quad \text{(C21)}$$

APPENDIX D: COMPUTATION OF FLOQUET MODES

The dynamics of a quantum system is described by the time-dependent TDSE,

$$i\hbar \frac{\partial}{\partial t}|\psi(t)\rangle = H(t)|\psi(t)\rangle. \quad \text{(D1)}$$

If $H(t + T) = H(t)$, then the Floquet theorem states that there exists solutions to Eq. (D1) called Floquet states given by

$$|u_\eta(t)\rangle = e^{-i\epsilon_\eta t/\hbar}|\phi_\eta(t)\rangle, \quad \text{(D2)}$$

where ϵ_η is a real-valued number called the quasienergy and $|\phi_\eta(t)\rangle$ is called the Floquet mode which has the same periodicity as the Hamiltonian, i.e., $|\phi_\eta(t + T)\rangle = |\phi_\eta(t)\rangle$.

On substituting Eq. (D2) in Eq. (D1), we get

$$\left(H(t) - i\hbar \frac{\partial}{\partial t}\right)|\phi_\eta(t)\rangle = \epsilon_\eta|\phi_\eta(t)\rangle. \quad \text{(D3)}$$

So, the quasienergies are eigenvalues of the Floquet quasienergy operator $(H(t) - i\hbar\frac{\partial}{\partial t})$ with Floquet modes as the eigenstates.

The Floquet modes can be expanded in the FD basis $\{|l\rangle\}$ (or any orthonormal basis) as

$$|\phi_\eta(t)\rangle = \sum_l c_{l,\eta}(t)|l\rangle, \tag{D4}$$

where $c_{l,\eta}(t) = \langle l|\phi_\eta(t)\rangle$ with $c_{l,\eta}(t) = c_{l,\eta}(t+T)$. Since $c_{l,\eta}(t)$ are time-periodic, they can be expanded in Fourier basis as

$$c_{l,\eta}(t) = \sum_{n=-\infty}^{\infty} c_{l,\eta}^n e^{in\omega t}, \tag{D5}$$

with $\omega = 2\pi/T$ being the angular frequency of the periodic drive. Using Eqs. (D4) and (D5), the Floquet modes can be rewritten as

$$|\phi_\eta(t)\rangle = \sum_{n=-\infty}^{\infty} \sum_l c_{l,\eta}^n |l\rangle e^{in\omega t}. \tag{D6}$$

Substituting Eq. (D6) in Eq. (D3), multiplying $e^{-in'\omega t}\langle l'|$ from left and time-averaging over a period T gives

$$\sum_{n=-\infty,l}^{\infty} \left(\frac{1}{T} \int_0^T \langle l'|H(t)|l\rangle e^{i(n-n')\omega t} dt + n\hbar\omega\delta_{n,n'}\delta_{l,l'} \right) c_{l,\eta}^n$$
$$= \epsilon_\eta c_{l',\eta}^{n'}. \tag{D7}$$

The above system of equations represents an infinite-dimensional matrix eigenvalue equation:

$$H_F \Phi_\eta = \epsilon_\eta \Phi_\eta, \tag{D8}$$

where H_F is the Floquet Hamiltonian matrix and Φ_η is its eigenvector corresponding to the quasienergy eigenvalue ϵ_η. The matrix elements of H_F and Φ_η are given by

$$\langle l', n'|H_F|l, n\rangle = \frac{1}{T} \int_0^T \langle l'|H(t)|l\rangle e^{i(n-n')\omega t} dt + n\hbar\omega\delta_{n,n'}\delta_{l,l'}, \tag{D9}$$

and $\Phi_\eta = (.. c_{l,\eta}^n ..)^{\mathcal{T}}$ where $\mathcal{T}$ stands for transpose. The eigenvalues are obtained numerically by truncating the matrix up to a certain order in n depending on the strength of the periodic drive. Once Φ_η is computed, the Floquet mode can be obtained by plugging the coefficients $\{c_{l,\eta}^n\}$ back into Eq. (D6).

APPENDIX E: TIME-EVOLVED STATE IN FLOQUET PICTURE

At $t = 0$, Eq. (D6) gives

$$|\phi_\eta(0)\rangle = \sum_l \left(\sum_{n'=-\infty}^{\infty} c_{l,\eta}^{n'} \right)|l\rangle. \tag{E1}$$

We drop the infinite summation limit of n' from this point as we consider only a finite $n_{\max}$. It can be shown that $\{|\phi_\eta(0)\rangle\}$ form a complete basis, i.e., $\sum_\eta |\phi_\eta(0)\rangle\langle\phi_\eta(0)| = 1$. Hence, if the system is initialized in a FD state, say $|i\rangle$, then

$$|\psi(0)\rangle = |i\rangle = \sum_\eta |\phi_\eta(0)\rangle\langle\phi_\eta(0)|i\rangle$$
$$= \sum_\eta \left(\sum_{n'} \left(c_{i,\eta}^{n'}\right)^* \right)|\phi_\eta(0)\rangle. \tag{E2}$$

To obtain the time-evolved state $|\psi(t)\rangle$, we use the Floquet time-evolution operator

$$U(t) = \mathcal{P}(t)e^{-i\mathcal{H}_F t/\hbar}, \tag{E3}$$

where $\mathcal{P}(t) = \mathcal{P}(t+T)$ is a time-periodic unitary operator [with $\mathcal{P}(0) = 1$] and $\mathcal{H}_F$ is a time-independent Hermitian operator called the Floquet Hamiltonian. The stroboscopic time-evolution operator is $U(T) = e^{-i\mathcal{H}_F T/\hbar}$. The application of $U(t)$ on $|\psi(0)\rangle$ gives

$$|\psi(t)\rangle = \sum_\eta \left(\sum_{n'} \left(c_{i,\eta}^{n'}\right)^* \right)\mathcal{P}(t)e^{-i\mathcal{H}_F t/\hbar}|\phi_\eta(0)\rangle. \tag{E4}$$

Since $|\phi_\eta(0)\rangle$ is an eigenstate of $\mathcal{H}_F$ [see Eq. (D8)] with eigenvalue ϵ_η, we get

$$|\psi(t)\rangle = \sum_\eta \left(\sum_{n'} \left(c_{i,\eta}^{n'}\right)^* \right)e^{-i\epsilon_\eta t/\hbar}\mathcal{P}(t)|\phi_\eta(0)\rangle$$
$$= \sum_\eta \left(\sum_{n'} \left(c_{i,\eta}^{n'}\right)^* \right)e^{-i\epsilon_\eta t/\hbar}|\phi_\eta(t)\rangle$$
$$= \sum_\eta \left(\sum_{n'} \left(c_{i,\eta}^{n'}\right)^* \right)\left(\sum_{l,n} c_{l,\eta}^n e^{-i(\epsilon_\eta - n\hbar\omega)t/\hbar} \right)|l\rangle, \tag{E5}$$

where we have used Eq. (D6) in the last step. Thus, the probability amplitude of finding the system in state $|f\rangle$ when initialized in state $|i\rangle$ is

$$\langle f|\psi(t)\rangle = \sum_\eta \left(\sum_{n'} \left(c_{i,\eta}^{n'}\right)^* \right)\left(\sum_n c_{f,\eta}^n e^{-i(\epsilon_\eta - n\hbar\omega)t/\hbar} \right). \tag{E6}$$

[1] G. Burkard, T. D. Ladd, A. Pan, J. M. Nichol, and J. R. Petta, Semiconductor spin qubits, Rev. Mod. Phys. **95**, 025003 (2023).

[2] A. Chatterjee, P. Stevenson, S. D. Franceschi, A. Morello, L. N. P.de, and F. Kuemmeth, Semiconductor qubits in practice, Nat. Rev. Phys. **3**, 157 (2021).

[3] D. D. Awschalom, L. C. Bassett, A. S. Dzurak, E. L. Hu, and J. R. Petta, Quantum spintronics: Engineering and manipulating atom-like spins in semiconductors, Science **339**, 1174 (2013).

[4] X. Zhang, H.-O. Li, G. Cao, M. Xiao, G.-C. Guo, and G. P. Guo, Semiconductor quantum computation, Nat. Sci. Rev. **6**, 32 (2019).

[5] B. E. Kane, A silicon-based nuclear spin quantum computer, Nature (London) **393**, 133 (1998).

[6] A. G. Fowler, M. Mariantoni, J. M. Martinis, and A. N. Cleland, Surface codes: Towards practical large-scale quantum computation, Phys. Rev. A **86**, 032324 (2012).

[7] D. Loss and D. P. DiVincenzo, Quantum computation with quantum dots, Phys. Rev. A **57**, 120 (1998).

[8] F. H. L. Koppens, C. Buizert, K. J. Tielrooij, I. T. Vink, K. C. Nowack, T. Meunier, L. P. Kouwenhoven, and L. M. K. Vandersypen, Driven coherent oscillations of a single electron spin in a quantum dot, Nature (London) **442**, 766 (2006).

[9] F. H. L. Koppens, K. C. Nowack, and L. M. K. Vandersypen, Spin echo of a single electron spin in a quantum dot, Phys. Rev. Lett. **100**, 236802 (2008).

[10] J. J. Pla, K. Y. Tan, J. P. Dehollain, W. H. Lim, J. J. Morton, D. N. Jamieson, A. S. Dzurak, and A. Morello, A single-atom electron spin qubit in silicon, Nature (London) **489**, 541 (2012).

[11] M. Veldhorst, J. C. C. Hwang, C. H. Yang, A. W. Leenstra, B. d. Ronde, J. P. Dehollain, J. T. Muhonen, F. E. Hudson, K. M. Itoh, A. Morello, and A. S. Dzurak, An addressable quantum dot qubit with fault-tolerant control-fidelity, Nat. Nanotechnol. **9**, 981 (2014).

[12] M. Veldhorst, C. H. Yang, J. C. C. Hwang, W. Huang, J. P. Dehollain, J. T. Muhonen, V. Simmons, A. Laucht, F. E. Hudson, K. M. Itoh, A. Morello, and A. S. Dzurak, A two-qubit logic gate in silicon, Nature (London) **526**, 410 (2015).

[13] Y. Kato, R. C. Myers, D. C. Driscoll, A. C. Gossard, J. Levy, and D. D. Awschalom, Gigahertz electron spin manipulation using voltage-controlled g-tensor modulation, Science **299**, 1201 (2003).

[14] G. Salis, Y. Kato, K. Ensslin, D. C. Driscoll, A. C. Gossard, and D. D. Awschalom, Electrical control of spin coherence in semiconductor nanostructures, Nature (London) **414**, 619 (2001).

[15] R. S. Deacon, Y. Kanai, S. Takahashi, A. Oiwa, K. Yoshida, K. Shibata, K. Hirakawa, Y. Tokura, and S. Tarucha, Electrically tuned g tensor in an InAs self-assembled quantum dot, Phys. Rev. B **84**, 041302(R) (2011).

[16] J. Pingenot, C. E. Pryor, and M. E. Flatté, Electric-field manipulation of the landé g tensor of a hole in an $In_{0.5}Ga_{0.5}As$/GaAs self-assembled quantum dot, Phys. Rev. B **84**, 195403 (2011).

[17] A. Ferrón, S. A. Rodriguez, S. S. Gómez, J. L. Lado, and J. Fernández-Rossier, Single spin resonance driven by electric modulation of the g-factor anisotropy, Phys. Rev. Res. **1**, 033185 (2019).

[18] M. P. Ladrière, T. Obata, Y. Tokura, Y.-S. Shin, T. Kubo, K. Yoshida, T. Taniyama, and S. Tarucha, Electrically driven single-electron spin resonance in a slanting Zeeman field, Nat. Phys. **4**, 776 (2008).

[19] R. Brunner, Y.-S. Shin, T. Obata, M. Pioro-Ladrière, T. Kubo, K. Yoshida, T. Taniyama, Y. Tokura, and S. Tarucha, Two-qubit gate of combined single-spin rotation and interdot spin exchange in a double quantum dot, Phys. Rev. Lett. **107**, 146801 (2011).

[20] J. Yoneda, K. Takeda, T. Otsuka, T. Nakajima, M. R. Delbecq, G. Allison, T. Honda, T. Kodera, S. Oda, Y. Hoshi, N. Usami, K. M. Itoh, and S. Tarucha, A quantum-dot spin qubit with

coherence limited by charge noise and fidelity higher than 99.9 percent, Nat. Nanotechnol. **13**, 102 (2018).

[21] D. M. Zajac, A. J. Sigillito, M. Russ, F. Borjans, J. M. Taylor, G. Burkard, and J. R. Petta, Resonantly driven CNOT gate for electron spins, Science **359**, 439 (2018).

[22] K. C. Nowack, F. H. L. Koppens, Y. V. Nazarov, and L. M. K. Vandersypen, Coherent control of a single electron spin with electric fields, Science **318**, 1430 (2007).

[23] S. N. Perge, S. M. Frolov, E. P. A. M. Bakkers, and L. P. Kouwenhoven, Spin–orbit qubit in a semiconductor nanowire, Nature (London) **468**, 1084 (2010).

[24] E. I. Rashba and A. L. Efros, Orbital mechanisms of electron-spin manipulation by an electric field, Phys. Rev. Lett. **91**, 126405 (2003).

[25] V. N. Golovach, M. Borhani, and D. Loss, Electric-dipole-induced spin resonance in quantum dots, Phys. Rev. B **74**, 165319 (2006).

[26] D. V. Bulaev and D. Loss, Electric dipole spin resonance for heavy holes in quantum dots, Phys. Rev. Lett. **98**, 097202 (2007).

[27] M. Brooks and G. Burkard, Electric dipole spin resonance of two-dimensional semiconductor spin qubits, Phys. Rev. B **101**, 035204 (2020).

[28] D. V. Khomitsky, L. V. Gulyaev, and E. Y. Sherman, Spin dynamics in a strongly driven system: Very slow Rabi oscillations, Phys. Rev. B **85**, 125312 (2012).

[29] A. V. Khaetskii and Y. V. Nazarov, Spin-flip transitions between Zeeman sublevels in semiconductor quantum dots, Phys. Rev. B **64**, 125316 (2001).

[30] V. N. Golovach, A. Khaetskii, and D. Loss, Phonon-induced decay of the electron spin in quantum dots, Phys. Rev. Lett. **93**, 016601 (2004).

[31] D. V. Bulaev and D. Loss, Spin relaxation and anticrossing in quantum dots: Rashba versus Dresselhaus spin-orbit coupling, Phys. Rev. B **71**, 205324 (2005).

[32] V. I. Fal'ko, B. L. Altshuler, and O. Tsyplyatyev, Anisotropy of spin splitting and spin relaxation in lateral quantum dots, Phys. Rev. Lett. **95**, 076603 (2005).

[33] S. I. Erlingsson and Y. V. Nazarov, Hyperfine-mediated transitions between a Zeeman split doublet in GaAs quantum dots: The role of the internal field, Phys. Rev. B **66**, 155327 (2002).

[34] A. V. Khaetskii, D. Loss, and L. Glazman, Electron spin decoherence in quantum dots due to interaction with nuclei, Phys. Rev. Lett. **88**, 186802 (2002).

[35] W. A. Coish and D. Loss, Hyperfine interaction in a quantum dot: Non-Markovian electron spin dynamics, Phys. Rev. B **70**, 195340 (2004).

[36] P. Becker, H.-J. Pohl, H. Riemann, and N. Abrosimov, Enrichment of silicon for a better kilogram, Phys. Status Solidi A **207**, 49 (2010).

[37] A. M. Tyryshkin, S. Tojo, J. J. L. Morton, H. Riemann, N. V. Abrosimov, P. Becker, H.-J. Pohl, T. Schenkel, M. L. W. Thewalt, K. M. Itoh, and S. A. Lyon, Electron spin coherence exceeding seconds in high-purity silicon, Nat. Mater. **11**, 143 (2012).

[38] K. Itoh, W. L. Hansen, E. E. Haller, J. W. Farmer, V. I. Ozhogin, A. Rudnev, and A. Tikhomirov, High purity isotopically enriched ^{70}Ge and ^{74}Ge single crystals: Isotope

separation, growth, and properties, J. Mater. Res. **8**, 1341 (1993).

[39] Y. Fang, P. Philippopoulos, D. Culcer, W. A. Coish, and S. Chesi, Recent advances in hole-spin qubits, Mater. Quantum. Technol. **3**, 012003 (2023).

[40] E. A. Chekhovich, M. M. Glazov, A. B. Krysa, M. Hopkinson, P. Senellart, A. Lemaitre, M. S. Skolnick, and A. I. Tartakovskii, Element-sensitive measurement of the hole-nuclear spin interaction in quantum dots, Nat. Phys. **9**, 74 (2013).

[41] J. Fischer, W. A. Coish, D. V. Bulaev, and D. Loss, Spin decoherence of a heavy hole coupled to nuclear spins in a quantum dot, Phys. Rev. B **78**, 155329 (2008).

[42] M. Vidal, M. V. Durnev, L. Bouet, T. Amand, M. M. Glazov, E. L. Ivchenko, P. Zhou, G. Wang, T. Mano, T. Kuroda, X. Marie, K. Sakoda, and B. Urbaszek, Hyperfine coupling of hole and nuclear spins in symmetric (111)-grown GaAs quantum dots, Phys. Rev. B **94**, 121302(R) (2016).

[43] J. H. Prechtel, A. V. Kuhlmann, J. Houel, A. Ludwig, S. R. Valentin, A. D. Wieck, and R. J. Warburton, Decoupling a hole spin qubit from the nuclear spins, Nat. Mater. **15**, 981 (2016).

[44] L. Zhang, J.-W. Luo, A. Saraiva, B. Koiller, and A. Zunger, Genetic design of enhanced valley splitting towards a spin qubit in silicon, Nat. Commun. **4**, 2396 (2013).

[45] D. V. Bulaev and D. Loss, Spin relaxation and decoherence of holes in quantum dots, Phys. Rev. Lett. **95**, 076805 (2005).

[46] G. Scappucci, C. Kloeffel, F. A. Zwanenburg, D. Loss, M. Myronov, J.-J. Zhang, S. D. Franceschi, G. Katsaros, and M. Veldhorst, The germanium quantum information route, Nat. Rev. Mater. **6**, 926 (2021).

[47] M. Lodari, A. Tosato, D. Sabbagh, M. A. Schubert, G. Capellini, A. Sammak, M. Veldhorst, and G. Scappucci, Light effective hole mass in undoped Ge/SiGe quantum wells, Phys. Rev. B **100**, 041304(R) (2019).

[48] J.-W. Luo, S.-S. Li, and A. Zunger, Rapid transition of the hole Rashba effect from strong field dependence to saturation in semiconductor nanowires, Phys. Rev. Lett. **119**, 126401 (2017).

[49] H. Watzinger, K. Kukučka, L. Vukušić, F. Gao, T. Wang, F. Schäffler, J.-J. Zhang, and G. Katsaros, A germanium hole spin qubit, Nat. Commun. **9**, 3902 (2018).

[50] N. W. Hendrickx, W. I. L. Lawrie, L. Petit, A. Sammak, G. Scappucci, and M. Veldhorst, A single-hole spin qubit, Nat. Commun. **11**, 3478 (2020).

[51] N. W. Hendrickx, D. P. Franke, A. Sammak, G. Scappucci, and M. Veldhorst, Fast two-qubit logic with holes in germanium, Nature (London) **577**, 487 (2020).

[52] K. Wang, G. Xu, F. Gao, H. Liu, R.-L. Ma, X. Zhang, Z. Wang, G. Cao, T. Wang, J.-J. Zhang, D. Culcer, X. Hu, H. W. Jiang, H.-O. Li, G.-C. Guo, and G.-P. Guo, Ultrafast coherent control of a hole spin qubit in a germanium quantum dot, Nat. Commun. **13**, 206 (2022).

[53] R. Winkler, Rashba spin splitting in two-dimensional electron and hole systems, Phys. Rev. B **62**, 4245 (2000).

[54] E. Marcellina, A. R. Hamilton, R. Winkler, and D. Culcer, Spin-orbit interactions in inversion-asymmetric two-dimensional hole systems: A variational analysis, Phys. Rev. B **95**, 075305 (2017).

[55] L. A. Terrazos, E. Marcellina, Z. Wang, S. N. Coppersmith, M. Friesen, A. R. Hamilton, X. Hu, B. Koiller, A. L. Saraiva,

D. Culcer, and R. B. Capaz, Theory of hole-spin qubits in strained germanium quantum dots, Phys. Rev. B **103**, 125201 (2021).

[56] A. Sarkar, Z. Wang, M. Rendell, N. W. Hendrickx, M. Veldhorst, G. Scappucci, M. Khalifa, J. Salfi, A. Saraiva, A. S. Dzurak, A. R. Hamilton, and D. Culcer, Electrical operation of planar Ge hole spin qubits in an in-plane magnetic field, Phys. Rev. B **108**, 245301 (2023).

[57] Y. Liu, J.-X. Xiong, Z. Wang, W.-L. Ma, S. Guan, J.-W. Luo, and S.-S. Li, Emergent linear Rashba spin-orbit coupling offers fast manipulation of hole-spin qubits in germanium, Phys. Rev. B **105**, 075313 (2022).

[58] E. L. Ivchenko, A. Y. Kaminski, and U. Rössler, Heavy-light hole mixing at zinc-blende (001) interfaces under normal incidence, Phys. Rev. B **54**, 5852 (1996).

[59] J.-W. Luo, G. Bester, and A. Zunger, Supercoupling between heavy-hole and light-hole states in nanostructures, Phys. Rev. B **92**, 165301 (2015).

[60] L. E. Golub and E. L. Ivchenko, Spin splitting in symmetrical SiGe quantum wells, Phys. Rev. B **69**, 115333 (2004).

[61] M. V. Durnev, M. M. Glazov, and E. L. Ivchenko, Spin-orbit splitting of valence subbands in semiconductor nanostructures, Phys. Rev. B **89**, 075430 (2014).

[62] J.-X. Xiong, S. Guan, J.-W. Luo, and S.-S. Li, Emergence of strong tunable linear Rashba spin-orbit coupling in two-dimensional hole gases in semiconductor quantum wells, Phys. Rev. B **103**, 085309 (2021).

[63] E. A. Rodriguez-Mena, J. C. Abadillo-Uriel, G. Veste, B. Martinez, J. Li, B. Sklénard, and Y.-M. Niquet, Linear-in-momentum spin orbit interactions in planar Ge/GeSi heterostructures and spin qubits, Phys. Rev. B **108**, 205416 (2023).

[64] J. C. Abadillo-Uriel, E. A. Rodriguez-Mena, B. Martinez, and Y.-M. Niquet, Hole-spin driving by strain-induced spin-orbit interactions, Phys. Rev. Lett. **131**, 097002 (2023).

[65] B. Martinez, J. C. Abadillo-Uriel, E. A. Rodriguez-Mena, and Y.-M. Niquet, Hole spin manipulation in inhomogeneous and nonseparable electric fields, Phys. Rev. B **106**, 235426 (2022).

[66] J. Orenstein, Ultrafast spectroscopy of quantum materials, Phys. Today **65**, 44 (2012).

[67] T. Kobayashi, Development of ultrashort pulse lasers for ultrafast spectroscopy, Photonics **5**, 19 (2018).

[68] A. Zong, B. R. Nebgen, S.-C. Lin, J. A. Spies, and M. Zuerch, Emerging ultrafast techniques for studying quantum materials, Nat. Rev. Mater. **8**, 224 (2023).

[69] J. M. Luttinger, Quantum theory of cyclotron resonance in semiconductors: General theory, Phys. Rev. **102**, 1030 (1956).

[70] A. Baldereschi and N. O. Lipari, Spherical model of shallow acceptor states in semiconductors, Phys. Rev. B **8**, 2697 (1973).

[71] H. W. van Kesteren, E. C. Cosman, W. A. J. A. van der Poel, and C. T. Foxon, Fine structure of excitons in type-II GaAs/AlAs quantum wells, Phys. Rev. B **41**, 5283 (1990).

[72] D. H. Kobe and K.-H. Yang, Gauge transformation of the time-evolution operator, Phys. Rev. A **32**, 952 (1985).

[73] M. Borhani, V. N. Golovach, and D. Loss, Spin decay in a quantum dot coupled to a quantum point contact, Phys. Rev. B **73**, 155311 (2006).

[74] D. Fernández-Fernández, J. P-Cortés, S. V. Liñán, and G. Platero, Photo-assisted spin transport in double quantum

dots with spin–orbit interaction, J. Phys. Mater. **6**, 034004 (2023).

[75] R. Moriya, K. Sawano, Y. Hoshi, S. Masubuchi, Y. Shiraki, A. Wild, C. Neumann, G. Abstreiter, D. Bougeard, T. Koga, and T. Machida, Cubic Rashba spin-orbit interaction of a two-dimensional hole gas in a strained-Ge/SiGe quantum well, Phys. Rev. Lett. **113**, 086601 (2014).